bioRxiv preprint doi: https://doi.org/10.1101/2021.02.28.433255; this version posted February 28, 2021. The copyright holder for this preprint (which was not certified by peer review) is the author/funder, who has granted bioRxiv a license to display the preprint in perpetuity. It is made available under aCC-BY-NC-ND 4.0 International license.

Alanine cross-feeding determines *Escherichia coli* colony growth dynamics

Francisco Díaz-Pascual[1], Martin Lempp[1], Kazuki Nosho[1], Hannah Jeckel[1,2], Jeanyoung K. Jo[3], Konstantin Neuhaus[1,2], Raimo Hartmann[1], Eric Jelli[1,2], Mads Frederik Hansen[1], Lars E.P. Dietrich[3], Hannes Link[1,4], and Knut Drescher[1,2,5,#].

[1] Max Planck Institute for Terrestrial Microbiology, Marburg, Germany.
[2] Department of Physics, Philipps-Universität Marburg, Marburg, Germany.
[3] Department of Biological Sciences, Columbia University, New York, NY, USA.
[4] Interfaculty Institute for Microbiology and Infection Medicine, University of Tübingen, Tübingen, Germany.
[5] Biozentrum, University of Basel, Basel, Switzerland.
[#] Correspondence to: knut.drescher@unibas.ch

Abstract

Bacteria commonly live in spatially structured assemblages encased by an extracellular matrix, termed biofilms. Metabolic activity of the cells inside biofilms causes gradients in local environmental conditions, which leads to the emergence of subpopulations with different metabolism. Basic information about the spatial arrangement of such metabolic subpopulations, as well as their interaction strength and interaction length scales are lacking, even for model systems like biofilms of *Escherichia coli* grown as colonies on agar-solidified media. Here, we use an unbiased approach based on temporal and spatial transcriptome and metabolome data during *E. coli* colony biofilm growth to identify many potential cross-feeding interactions. The strongest signature for cross-feeding in these data was displayed by alanine metabolism, and we discovered that alanine is indeed a cross-fed metabolite between two spatially segregated subpopulations: Alanine is secreted primarily *via* the transporter AlaE by anaerobically growing cells that are saturated with carbon and nitrogen, whereas alanine is utilized as a carbon and nitrogen source *via* DadA and DadX in the aerobic nutrient-deprived region at mid-height of the colony. We demonstrate that alanine cross-feeding influences cellular viability and growth in the cross-feeding-dependent region, which shapes the overall colony morphology. More generally, our methodology enables an unbiased path to the identification and characterization of spatially organized metabolic interactions in microbial communities, which are essential for understanding community structure and stability.

Introduction

After bacterial cell division on surfaces, daughter cells often remain in close proximity to their mother cells. This process leads to closely packed populations with spatial structure, which are often held together by an extracellular matrix. Such spatially structured assemblages, called biofilms (1), are estimated to be the most abundant form of microbial life on Earth (2). The metabolic activity of cells inside these dense populations leads to spatial gradients of oxygen, carbon and nitrogen sources, as well as many other nutrients and waste products (3–5). Cells in different locations within these assemblages therefore inhabit distinct microenvironments. Physiological adaptation to microenvironmental conditions results in spatially segregated subpopulations of cells with different metabolism (5). Bacterial growth into spatially structured communities and metabolic activity of the constituent cells therefore naturally lead to physiological differentiation (4).

When two or more subpopulations coexist in spatial proximity, some metabolites produced by one of the subpopulations may reach another subpopulation and be utilized by it, either as electron acceptors for energy metabolism, or as carbon and nitrogen sources in a process termed cross-feeding (4, 6–12). Several cross-feeding interactions have been documented between phenotypic subpopulations of isogenic strains in liquid cultures without spatial structure (13–15) and subpopulations between genetically different microorganisms in spatially structured communities (7, 16–21), yet only a few studies have investigated cross-feeding in isogenic species with spatial structure. These studies used colony models to focus on cross-feeding interactions that were assumed to take place, and found that *Bacillus subtilis* can differentially produce and consume ammonium (22), *Escherichia coli* can cross-feed acetate (23–25), and *Pseudomonas aeruginosa* can cross-feed lactate (26). Recent computational analyses predict that cross-feeding interactions could be much more wide-spread, and

bioRxiv preprint doi: https://doi.org/10.1101/2021.02.28.433255; this version posted February 28, 2021. The copyright holder for this preprint (which was not certified by peer review) is the author/funder, who has granted bioRxiv a license to display the preprint in perpetuity. It is made available under aCC-BY-NC-ND 4.0 International license.

that dozens of metabolites could be involved (6, 27, 28). Such predictions have not yet been tested, and unbiased approaches aimed at identifying important cross-feeding interactions are lacking. Systematic experimental studies of cross-feeding in biofilms are technically challenging as these systems change in space and time on microscopic and mesoscopic length scales, and large parts of the biofilms are anaerobic, which prevents the use of bright fluorescent proteins (29). Therefore, the extent of cross-feeding and metabolic dependencies of subpopulations in biofilms has remained unclear, even for simple model systems like single-species colonies on agar plates.

To obtain insights into the spatial metabolism inside biofilms that are unbiased by previously predicted or speculated interactions, we acquired metabolomic and transcriptomic data with temporal and spatial resolution during the development of *E. coli* colony biofilms on a defined minimal medium that was solidified by agar. By combining metabolome and transcriptome data, we discovered spatially and temporally regulated secretion and consumption of alanine, which can be used as a good nitrogen source or a poor carbon source by *E. coli*. Secretion of alanine occurs in the part of the anaerobic region of the colony where the carbon and nitrogen sources are abundant. The secreted alanine is then consumed in a part of the aerobic region of the colony, where glucose and ammonium from the minimal medium are lacking. We show that alanine cross-feeding has important consequences for cellular viability, growth, and colony morphology. These results demonstrate that unbiased approaches that combine temporal and spatial transcriptomes with metabolomes and microscopy are a powerful tool for understanding metabolic interactions in microbial communities.

Results and discussion

Colony growth transitions and global metabolic changes. To investigate the spatial organization of metabolism inside *E. coli* colonies, we first characterized the basic colony growth dynamics and morphology on solid M9 minimal medium, which contained glucose and ammonium as the sole carbon and nitrogen sources, respectively (Fig. 1A). For all measurements performed on colonies, including microscopy-based measurements, the colonies were grown on top of filter membranes that were placed on M9 agar (SI Appendix, Fig. S1A). These membranes enabled rapid sampling of the colonies for transcriptome and metabolome analyses. When we grew *E. coli* wild type colonies, we observed motility on the filter membranes on M9 agar, which led to heterogeneous colony development and an asymmetric colony morphology (SI Appendix, Fig. S1B). Therefore, a strain lacking flagella due to the deletion of the flagellin (Δ*fliC*) was used as the parental strain for all following experiments, which resulted in highly reproducible and axially symmetric colony morphologies (SI Appendix, Fig. S1C). Colonies generally displayed two growth phases: initially, colonies grew exponentially in volume, height, and diameter for up to ~24 h, followed by linear growth (Fig. 1A,B). This transition in colony growth dynamics has previously been hypothesized to be caused by a change in metabolism due to altered nutrient penetration and consumption for colonies above a certain size (30, 31).

To characterize the phenotypic changes that occur during colony growth, we performed time-resolved whole-colony transcriptome measurements (Fig. 1C and SI Appendix, Fig. S2A). The transcriptomes revealed a major change after 24 h growth (Fig. 1C), which reflects the change in growth dynamics that was apparent in the morphological parameters (Fig. 1B). After 72 h of growth, 966 genes of 4,231 detected genes were differentially expressed in comparison to 12 h ($\log_2$-fold changes >1 or <-1, and FDR-adjusted p-value <0.05). The whole-colony transcriptomes also showed that biofilm matrix biosynthesis genes are expressed continuously during colony growth (SI Appendix, Fig. S3). Furthermore, the transcriptomes revealed that mixed acid fermentation and tricarboxylic acid (TCA) cycle pathways were differentially regulated after 24 h of growth (SI Appendix, Fig. S4A,C). These results are consistent with the hypothesis that above a certain colony size, which is apparently reached between 24-32 h, the consumption of oxygen by cells in the outer region of the colony causes an anoxic region inside the colony.

Although it is commonly assumed that *E. coli* subpopulations cross-feed acetate (23–25, 32), the temporal transcriptomes did not reveal strong regulation of acetate metabolism during colony growth. Lactate, formate, and succinate biosynthesis, however, displayed interesting signatures that could be indicative of carbon cross-feeding (SI Appendix, Fig. S4A). Apart from these metabolites, we noticed interesting patterns in the expression of amino acid pathways. For amino acids to be cross-fed, they need to be exported and imported by the cells. While gene expression levels for some amino acid transporters remained unchanged during colony growth, several were >2-fold up- or down-regulated after 24 h or 32 h of growth (Fig. 1D). However, the gene coding for the alanine exporter *alaE* (33) showed strong expression changes (~50-fold increase) in 72-h-colonies relative to 12-h-colonies (Fig. 1D). Using mass spectrometry, we then measured the amino acid profiles in the colony, normalized by

bioRxiv preprint doi: https://doi.org/10.1101/2021.02.28.433255; this version posted February 28, 2021. The copyright holder for this preprint (which was not certified by peer review) is the author/funder, who has granted bioRxiv a license to display the preprint in perpetuity. It is made available under aCC-BY-NC-ND 4.0 International license.

the colony biomass. All amino acid abundances displayed a similar pattern during colony growth – except for alanine, which had a peak abundance at 32 h (Fig. 1E,F, SI Appendix, Fig. S2B and Fig. S5).

Thus, both transcriptome and metabolome data suggest a unique change of alanine metabolism during colony growth, which led us to investigate its role in *E. coli* colonies. We hypothesized that alanine is a cross-fed metabolite in *E. coli* colonies and that this cross-feeding is the result of spatially organized metabolic differentiation. This hypothesis was investigated as described below.

Spatial regulation of alanine transport and degradation. Cross-feeding of alanine would require alanine-secreting and alanine-consuming populations. In order to identify if such subpopulations are present, we developed a method to measure transcriptomes with spatial resolution in the colonies. The method is based on the oxygen-dependence of chromophore maturation of many fluorescent proteins, such as mRuby2 (29, 34). Using a strain that constitutively expresses mRuby2 from a chromosomal locus, we observed for 72-h-colonies that only the air-facing region of the colony was fluorescent. A quantification of the mRuby2 fluorescence showed a slightly steeper decrease of fluorescence in the horizontal *xy*-direction into the colony, compared with the vertical *z*-direction (Fig. 2A). When using an oxygen microsensor to directly measure oxygen levels inside the colony (35) in the *z*-direction, we determined that the mRuby2 fluorescence was a reliable indicator of oxygen levels (Fig. 2A). During colony growth, the fraction of fluorescent cells in the colony decreased (insert in Fig. 2B), ultimately leading to a thin layer of fluorescent cells in the air-facing part of the colony (Fig. 2B). To eliminate the possibility that the observed fluorescence profile was due to microscopy imaging artefacts, such as insufficient laser penetration into the colony, we disrupted 72-h-colonies and immediately imaged the resulting, well-separated single cells. In these measurements, only some cells displayed fluorescence (SI Appendix, Fig. S6A), which, together with the fact the mRuby2 fluorophore maturation time is 150 min (34), confirms that the fluorescence gradient we observed in Fig. 2B is not an imaging artefact. Furthermore, since the oxygen gradient in the colony should be created by oxygen consumption (5), it should disappear when metabolic processes that consume oxygen are prevented. Indeed, when we moved a filter membrane carrying the colonies to an M9 agar plate lacking glucose, molecular oxygen penetrated throughout the colony, resulting in mRuby2 proteins located in the former anaerobic region to become fluorescent (SI Appendix, Fig. S6B,C).

To obtain spatial transcriptomes, we then separated colonies grown for 72 h into individual cells, fixed them with formaldehyde (which prevents mRuby2 fluorophore maturation), followed by fluorescence-activated cell sorting (FACS) to separate the aerobic (fluorescent) and anaerobic (not fluorescent) populations (Fig. 2C and SI Appendix, Fig. S7). The resulting two cell populations were then analyzed using RNA-seq. The spatial transcriptome comparison showed that, as expected, genes involved in the TCA cycle and mixed acid fermentation were differentially expressed between the inner and outer regions of the colony (SI Appendix, Fig. S4B,D). This result demonstrates that the method successfully separated the fermenting population inside the colonies from the respiring population in the outer layer, which serves as a qualitative verification of the experimental methodology.

In both the temporally and spatially resolved transcriptomes, we observed changes in alanine transport and degradation, but not in alanine biosynthesis (Fig. 2D,E; a schematic diagram of alanine metabolism pathways is shown in the SI Appendix, Fig. S8). In particular, the expression of the primary alanine exporter *alaE* was significantly up-regulated in the inner (non-fluorescent) region of the colony, compared with the outer (fluorescent) region (Fig. 2E). Alanine conversion into pyruvate and ammonium was also spatially regulated. Two pathways for converting alanine to pyruvate are known: The reversible conversion by enzymes involved in the alanine biosynthetic pathways, and the irreversible conversion mediated by the *dadAX* operon (SI Appendix, Fig. S8B). The latter encodes a racemase (*dadX*) and a dehydrogenase (*dadA*) (36). In colonies grown for 72 h, the expression of the *dadAX* operon was down-regulated in the inner region, compared with the outer region (Fig. 2E). In addition, *dadAX* expression was up-regulated in the whole-colony temporal transcriptomes (6-fold for *dadA* and 5-fold for *dadX*) when comparing 72-h-colonies to 12-h-colonies (Fig. 2D). These results indicate that colonies globally up-regulate alanine export and degradation during development and that the anaerobic region of the colony likely exports alanine, while the aerobic region likely converts alanine into pyruvate and ammonium.

Alanine is exported in anoxic conditions and can be used as a carbon and nitrogen source. If alanine is cross-fed in colonies, it must be secreted in microenvironments found within the colony – the spatial transcriptomes indicate that this occurs in the anaerobic region. We therefore explored under which combination of carbon/nitrogen/oxygen availability *E. coli* secretes alanine in liquid conditions.

bioRxiv preprint doi: https://doi.org/10.1101/2021.02.28.433255; this version posted February 28, 2021. The copyright holder for this preprint (which was not certified by peer review) is the author/funder, who has granted bioRxiv a license to display the preprint in perpetuity. It is made available under aCC-BY-NC-ND 4.0 International license.

Mass spectrometry measurements from culture supernatants clearly showed that alanine is only secreted under anoxic conditions with glucose and ammonium (Fig. 3A). This environment corresponds to the anaerobic base of the colony, where cells are in contact with the glucose- and ammonium-rich M9 agar, suggesting that alanine is secreted in that region, which is consistent with the spatial transcriptome results.

Cross-feeding of alanine requires that, besides being secreted, alanine can also be utilized by other cells. In order to investigate whether extracellular alanine can function as a carbon or nitrogen source, we replaced either glucose or ammonium by alanine in the liquid M9 medium (Fig. 3B,C). We found that exogenous alanine can be utilized as a poor carbon source, but as a good nitrogen source, which further supports the hypothesis that alanine is cross-fed in colonies.

Bacterial survival in the aerobic region of the colony is influenced by alanine export and consumption. To determine how interference with alanine export and consumption affects colony growth, we created individual and combinatorial deletions of all known alanine transport and degradation genes. None of these deletions affected the growth rates in liquid culture, or caused clear phenotypes in colony height or radius after 72 h of incubation on M9 agar (SI Appendix, Fig. S9). However, the mutants displayed substantial differences when we measured the fraction of dead cells in the aerobic region (Fig. 4A and SI Appendix, Fig. S10), using a fluorescent nucleic acid stain that can only penetrate the disrupted membranes of dead cells (SYTOX Green). We limited our measurements to the air-facing aerobic region of the colony, because in this region the SYTOX Green fluorescence can be reliably quantified without artefacts that may occur deeper inside the colony due to poor laser penetration. We observed that all colonies displayed a low fraction of dead cells at the bottom edges of the colony, but cell death increased towards the very top of the colony. Interestingly, the aerobic region at around 50% of the maximum colony height displayed increased cell death when cells carried the Δ*alaE*Δ*dadAX* deletion (Fig. 4A), which is a strain that should have a strongly reduced capability for alanine cross-feeding.

To determine if the increased cell death displayed by the Δ*alaE*Δ*dadAX* mutants could be caused by impaired alanine cross-feeding, we first measured the extracellular alanine concentration in colonies of the relevant mutants using mass spectrometry (Fig. 4B). Mutants incapable of the major alanine degradation pathway (Δ*dadAX*) displayed substantially higher extracellular alanine than cells that are impaired for alanine secretion as well (Δ*alaE*Δ*dadAX*). Although amino acid transporters can often function as both importers and exporters, these measurements indicate that AlaE acts as an alanine exporter inside colonies. The parental strain and the Δ*alaE* mutant displayed similarly low extracellular alanine levels, close to the detection limit of our mass spectrometry technique. Interestingly, and consistent with the results of Katsube *et al.* (37), the presence of extracellular alanine in colonies of the Δ*alaE* and Δ*alaE*Δ*dadAX* mutants indicates that another mechanism for alanine export might exist that is currently unknown.

For cells that lack both the major alanine exporter AlaE and the major alanine degradation pathway *via* DadA and DadX, we hypothesized that the presence of extracellular alanine might lead to an accumulation of intracellular alanine to toxic levels. It has previously been shown that excess levels of intracellular alanine can inhibit growth (38). Indeed, we observed that all strains show a decreased growth rate in liquid media containing high levels of alanine, yet strains carrying the Δ*alaE*Δ*dadAX* mutation were much more sensitive to exogenously added alanine than the parental strain (Fig. 4C). This result was not due to unspecific effects of alanine (such as osmolarity changes), because no significant differences between the mutants and the parental strain were observed when serine was added exogenously instead of alanine (SI Appendix, Fig. S11). Therefore, extracellular alanine can modulate bacterial growth rates, particularly for strains that are deficient in alanine cross-feeding (Δ*alaE*Δ*dadAX*).

Since colonies can accumulate alanine in their extracellular space (Fig. 4B) and their growth rate can be reduced by extracellular alanine (Fig. 4C), we hypothesized that the increased cell death in the aerobic region of the Δ*alaE*Δ*dadAX* colonies (Fig. 4A) is due to the accumulation of toxic extracellular alanine levels in this region, which arise from the impaired cross-feeding of this strain. To test this hypothesis, we measured cell viability for the mutants in liquid cultures with and without exogenous alanine during mid-exponential phase and in stationary phase. We found that in the presence of alanine, Δ*alaE*Δ*dadAX* mutants displayed higher cell death than the parental strain, which was particularly strong in stationary phase conditions (Fig. 4D). If cells can still export alanine (Δ*dadAX*) or still degrade alanine (Δ*alaE*), cell viability is significantly improved in the presence of extracellular

bioRxiv preprint doi: https://doi.org/10.1101/2021.02.28.433255; this version posted February 28, 2021. The copyright holder for this preprint (which was not certified by peer review) is the author/funder, who has granted bioRxiv a license to display the preprint in perpetuity. It is made available under aCC-BY-NC-ND 4.0 International license.

alanine, compared with the Δ*alaE*Δ*dadAX* mutant. We speculate that the exponentially growing cultures resembled the aerobic periphery at the base of the colony that is in contact with glucose and ammonium, whereas the stationary phase cultures resemble the aerobic region above, which is nutrient depleted if no cross-feeding is present.

Together, these results support the hypothesis that extracellular alanine which accumulates due to impaired cross-feeding causes the increased cell death in Δ*alaE*Δ*dadAX* mutant colonies. Alanine cross-feeding could therefore have an important effect for the aerobic region above the nutrient-rich base of the colony.

Alanine cross-feeding influences colony morphology. If alanine that is secreted in the anaerobic base of the colony is consumed in aerobic higher regions of the colony, alanine should serve as a carbon and nitrogen source and support growth in this region. From measurements of the colony height and maximum diameter for mutants impaired in cross-feeding (SI Appendix, Fig. S9), we know that alanine cross-feeding does apparently not matter at the aerobic top of the colony, and not in the aerobic respiration region at the base of the colony. We therefore investigated effects of alanine cross-feeding on cellular growth in the aerobic region at mid-height, where the fraction of dead cells was highest for the Δ*alaE*Δ*dadAX* mutants (Fig. 4A). Measurements of the colony morphology showed that Δ*alaE*Δ*dadAX* and Δ*alaE* mutants displayed a decreased colony curvature in the relevant region, in comparison to the parental strain (Fig. 5A,B). The "bulge" of the parental colonies suggests that this region may grow due to alanine cross-feeding. This interpretation is consistent with recent simulations of colony growth without cross-feeding, which resulted in nearly conical colony shapes with triangular *xz*-cross sections (30). To further experimentally investigate cellular growth in this mid-height aerobic region, we measured the fluorescence ratio of an unstable version of the superfolder GFP (39) and the long-lived mRuby2, both of which were expressed constitutively using the same P_{tac} promoter. The ratio of these fluorescent proteins serves as a measure of the cellular growth rate (SI Appendix, Fig. S12). These measurements showed that the parental strain grows faster in the mid-height aerobic region than the cross-feeding impaired Δ*alaE*Δ*dadAX* mutant (Fig. 5C), which further supports the hypothesis that this region relies on alanine as a carbon and nitrogen source.

Model for alanine cross-feeding in colony biofilms. The gradients of glucose, ammonium, and oxygen availability inside the *E. coli* colonies lead to the emergence of metabolic subpopulations. We propose that for colonies grown for 72 h in our system, two of these subpopulations interact through a cross-feeding of alanine, as summarized in the schematic model shown in Fig. 5D. Cells at the bottom periphery of the colony (red region in Fig. 5D) have access to molecular oxygen, glucose and ammonium, and perform aerobic respiration (23, 40). Cells at the bottom center of the colony (orange region in Fig. 5D) are anaerobic yet they have access to glucose and ammonium from the agar medium. These cells ferment glucose and secrete alanine primarily *via* AlaE. Secreted alanine diffuses through the colony and can eventually be converted into biomass by aerobic nutrient-deficient cells (green region in Fig. 5D). Alanine consumption in the aerobic top of the colony is irrelevant, perhaps because the extracellular alanine is consumed before it reaches this region.

Conclusion

For *E. coli* colonies grown on agar-solidified medium, and for bacterial communities in general, spatially organized metabolite cross-feeding is likely a ubiquitous process that is poorly understood. It is unclear how many subpopulations are involved, which metabolites they cross-feed, and on which length and time scales these interactions take place. In this study, we employed an unbiased approach based on temporal and spatial transcriptomes and metabolomes to reveal that a multitude of amino acids and mixed acid fermentation pathways display profiles that are consistent with cross-feeding. Particularly strong regulation was displayed by alanine metabolism, and we showed that alanine is a cross-fed metabolite inside *E. coli* colonies, between at least two spatially segregated subpopulations, with an interaction length scale of tens of microns. Alanine consumption supports growth in the cross-feeding-dependent region of the colony, and alanine consumption also has a detoxification effect by reducing otherwise inhibitory levels of extracellular alanine. Although many amino acid exporters have been described for *E. coli* (38, 41, 42), their functions have remained elusive under regular physiological conditions. Our data now reveal a population-level function for the alanine exporter AlaE during colony growth. Many aspects of metabolism in biofilms are still unknown, yet spatial and temporal analyses of metabolite profiles and transcriptome data provide the possibility to discover new metabolic interactions, and more generally understand the interactions and stability of microbial communities.

bioRxiv preprint doi: https://doi.org/10.1101/2021.02.28.433255; this version posted February 28, 2021. The copyright holder for this preprint (which was not certified by peer review) is the author/funder, who has granted bioRxiv a license to display the preprint in perpetuity. It is made available under aCC-BY-NC-ND 4.0 International license.

Acknowledgements

We are grateful to Thorben Schramm and Nicole Paczia for performing additional metabolite measurements, and Alexa Price-Whelan for comments on the manuscript. We also thank Miriam Bayer, Praveen K. Singh, Daniel Rode, Lucia Vidakovic, S. Vaidya, and all members of the Drescher lab for their comments and fruitful discussions. This work was supported by grants from the European Research Council (StG-716734), Deutsche Forschungsgemeinschaft (SFB987 and DR 982/5-1), Minna James Heineman Foundation, Bundesministerium für Bildung und Forschung (TARGET-Biofilms), Max Planck Society, and the Swiss National Science Foundation NCCR "AntiResist" (to K.D.), and an NSF CAREER award and NIH/NIAID grant R01AI103369 (to L.E.P.D.).

Authors Contributions

F.D.-P. and K.D. designed experiments and analyzed data. F.D.-P. performed growth and microscopy-based experiments. F.D-P., M.L., and H.L. designed and performed metabolomic experiments. Ka.No. designed and performed transcriptome experiments. H.J., R.H. and E.J. developed and performed image analysis. J.K.J. and L.E.P.D. designed and performed oxygen measurements. Ko.Ne. and R.H. developed microscope control and imaging techniques. M.F.H. generated strains. F.D.-P. and K.D. created the figures and wrote the manuscript with input from all authors. All authors made important conceptual contributions to the project and the interpretation of results, often in group discussions. K.D. supervised and coordinated the project.

Materials and Methods

Strains, strain construction, and media. All *E. coli* strains used in this study are derivatives of the *E. coli* K-12 AR3110 strain (43). For the construction of plasmids and bacterial strains, standard molecular biology techniques were applied (44), using enzymes purchased from New England Biolabs or Takara Bio. All AR3110 derivatives carried a constitutively expressed fluorescent protein expression system (based on the P_{tac} promoter without the *lac* operator) inserted in the chromosome at the *attB* site. To generate chromosomal deletions, the lambda red system was used to replace the target region with an antibiotic cassette flanked by FRT sites. Then, the Flp-FRT recombination system was utilized to remove the antibiotic resistance cassette. To insert the unstable fluorescent protein sfGFP(ASV) (39) expressed under the control of the P_{tac} promoter (without the *lac* operator) and a chloramphenicol cassette flanked by FRT sites into the Tn7 insertion site, we used the protocol described by Choi *et.al.* (45). After the fragment was inserted, the chloramphenicol resistance cassette was removed using the Flp-FRT recombination system. All strains, plasmids, and oligonucleotides that were used in this study are listed in the SI Appendix, Table S1, Table S2, and Table S3, respectively.

Cultures were grown in LB-Miller medium (10 g L^{-1} NaCl, 10 g L^{-1} tryptone, 5 g L^{-1} yeast extract) for routine culture and cloning, or in M9 minimal salts medium supplemented with 5 g L^{-1} D-glucose (which we refer to as "M9 medium" throughout the article for simplicity). The M9 minimal salts medium consisted of the following components: 42.3 mM Na_2HPO_4 (Carl Roth P030.2), 22 mM KH_2PO_4 (Carl Roth 3904.1), 11.3 mM $(NH_4)_2SO_4$ (Carl Roth 3746.2), 8.56 mM NaCl (Carl Roth HN00.2), 0.1 mM $CaCl_2$ (Sigma-Aldrich C5670), 1 mM $MgSO_4$, (Sigma-Aldrich M2643), 60 µM $FeCl_3$ (Sigma-Aldrich 31332), 2.8 µM thiamine-HCl (Sigma-Aldrich T4625), 6.3 µM $ZnSO_4$ (Sigma-Aldrich Z0251), 7 µM $CuCl_2$ (Sigma-Aldrich 307483), 7.1 µM $MnSO_4$ (Sigma-Aldrich M8179), 7.6 µM $CoCl_2$ (Carl Roth 7095.1). M9 agar plates were made using 8 mL of M9 medium (as defined above) with 1.5 % w/v agar-agar, aliquoted into petri dishes with 35 mm diameter and 10 mm height (Sarstedt 82.1135.500).

Colony biofilm growth. Cultures were inoculated from frozen glycerol stocks kept at -80 °C into LB-Miller medium with kanamycin (50 µg mL^{-1}) and grown for 5 h at 37 °C with shaking at 220 rpm. At this point, 1 µL of the culture was inoculated into 5 mL of M9 medium inside a 100-mL-Erlenmeyer flask and grown at 37 °C with shaking at 220 rpm for 16-22 h. The cultures were continuously kept in exponential phase by regular back-dilutions, with optical density at 600 nm (OD_{600}) always below 0.6. Aliquots from these cultures were passed through a sterile 0.45 µm pore size polyvinylidene fluoride membrane filter of diameter 5 mm, unless stated otherwise. High-resolution confocal fluorescence microscopy showed that this treatment resulted in spatially well-separated single cells on the filter membrane. Using clean and sterile stainless steel tweezers, these filter membranes carrying the cells were immediately placed directly onto M9 agar plates and incubated at 37 °C for up to 72 h.

Microscopy. All imaging was performed using a Yokogawa spinning disk confocal unit mounted on a Nikon Ti-E inverted microscope. A Nikon 40x air extra-long working distance objective with numerical

bioRxiv preprint doi: https://doi.org/10.1101/2021.02.28.433255; this version posted February 28, 2021. The copyright holder for this preprint (which was not certified by peer review) is the author/funder, who has granted bioRxiv a license to display the preprint in perpetuity. It is made available under aCC-BY-NC-ND 4.0 International license.

aperture (NA) 0.60 was used for all imaging, except for mutant screening (SI Appendix, Fig. S9) where a 4x air objective (NA 0.13, Nikon) was used, and single-cell imaging (SI Appendix, Fig. S6A) were a 100x oil objective (NA 1.45, Nikon) was used. All imaging was done inside a microscope incubator kept at 37 °C. Instead of imaging through the filter, colonies were imaged facing down and the Petri dish lid was removed (SI Appendix, Fig. S1A). To maintain a high humidity and avoid evaporation of the M9 agar, the space between the microscope objective and the petri dish was sealed with flexible plastic foil. To avoid condensation on the objective, the objective was heated using an objective heater at 37 °C.

Colony detection and biovolume measurements with adaptive microscopy. In preliminary experiments, we observed that colony growth of the wild type *E. coli* strain AR3110 resulted in heterogeneous shapes (SI Appendix, Fig. S1B, C) that were caused by flagella-based motility of cells on the filter membranes in the very early stages of incubation. To avoid the effects caused by cellular motility during early colony growth, all subsequently experiments were performed using a strain that lacks the flagellin FliC (Δ*fliC*), which we used as parental strain in this study. This strain was incapable of swimming motility, and the resulting colonies were highly reproducible in shape and highly symmetric (Fig. 1B and SI Appendix, Fig. S1B, C).

To determine the biomass of colonies, the colonies were grown on filter membranes on M9 agar as explained above, but with the addition of 0.2 µm dark red fluorescent beads (Invitrogen, F8807) to the bacterial suspension prior to filtering. This resulted in far-red fluorescent beads being located on the filter in addition to the red fluorescent cells. Using adaptive microscopy (46) these beads were used to find the correct focal plane for imaging of the bacterial cells (or base of the colonies). After 12 h, 18 h, 24 h, 32 h, 42 h, 48 h, 60 h, and 72 h of colony growth, the colonies were imaged in 3D using confocal microscopy. All colonies on the membrane filter were imaged using an adaptive microscopy approach (46) as follows: The whole filter was scanned using 2D imaging, followed by an identification of all colonies on the filter, followed by a high-resolution 3D imaging of each colony. From the scans of the whole filter, the number of colonies was determined. From the 3D images of the colonies, the biovolume was calculated. To obtain the biovolume, the outline of the colony was identified by thresholding the image gradient in each *z*-slice. The convex area of this binary image was then used as a measure for the biomass present in this plane such that summation over all slices followed by multiplication with the appropriate μm^3/voxel calibration yielded the biovolume of each colony.

Liquid growth assays. Cultures were inoculated from -80 °C frozen stocks into LB-Miller media and grown for 5 h at 37 °C with shaking at 220 rpm. Each culture was back-diluted 5,000-fold into 5 mL of M9 medium inside a 100-mL-Erlenmeyer flask, and grown at 37 °C with shaking at 220 rpm. At an OD_{600} of 0.3 each culture was washed 3 times in M9 minimal salts medium (lacking glucose and ammonium) and resuspended in the same volume of the medium of interest. These bacterial suspensions were diluted 10-fold and transferred into a 96-well plate (Sarstedt, 82.1581.001), and incubated at 37 °C with shaking in a microtiter plate reader (Epoch2, Biotek). The resulting growth curve data was analysed using Matlab (version R2019b, Mathworks).

To simultaneously measure OD_{600} and the ratio between unstable GFP (with the ASV-tag) and mRuby2 as a function of time (Fig. S12), strain KDE2937 was inoculated from a -80 °C frozen stock into LB-Miller media and grown for 5 h at 37 °C with shaking at 220 rpm. The culture was then back-diluted 5,000-fold into 5 mL of M9 medium inside a 100-mL Erlenmeyer flask and grown for 16 h. This culture was used to inoculate 75 mL of M9 medium inside a 1-L Erlenmeyer flask with an adjusted OD_{600} of 0.05. This culture was grown at 37°C with shaking at 220 rpm. Aliquots of the culture were taken every 30 min, to measure the OD_{600} and to determine the ratio between unstable GFP (with the ASV-tag) and mRuby2 using microscopy. To image the aliquots, they were placed between a cover slip and a M9 agar pad and imaged as described in the microscopy methods section.

Measurement of extracellular alanine in liquid culture supernatants. Cultures were inoculated from frozen -80 °C stocks into LB-Miller media with kanamycin (50 µg mL^{-1}) and grown for 5 h at 37 °C with shaking at 220 rpm. The cultures were then back-diluted 5,000-fold into 5 mL of M9 medium inside a 100-mL-Erlenmeyer flask and incubated at 37 °C with shaking at 220 rpm. These cultures were kept in exponential phase by regular back-dilutions, with optical density at 600 nm (OD_{600}) always below 0.6. At an OD_{600} of 0.3 the cultures were centrifuged at 14,000 g for 2 min and the supernatant was removed. To investigate aerobic growth conditions, the pellets were suspended in M9 minimal salts medium supplemented with glucose and the OD_{600} was adjusted to 0.1 by dilution. For aerobic starvation conditions, the pellets were suspended in same volume of M9 medium lacking ammonium but including glucose, M9 medium lacking glucose but including ammonium, or M9 medium lacking both glucose and

bioRxiv preprint doi: https://doi.org/10.1101/2021.02.28.433255; this version posted February 28, 2021. The copyright holder for this preprint (which was not certified by peer review) is the author/funder, who has granted bioRxiv a license to display the preprint in perpetuity. It is made available under aCC-BY-NC-ND 4.0 International license.

ammonium. The cultures were then placed into 100-mL-Erlenmeyer flasks at 37 °C with shaking at 220 rpm as before. To investigate anaerobic conditions, the pellets were suspended in the same media as described above, but the resulting cultures were transferred into a closed 15-mL-conical centrifuge tube (Sarstedt, 62.554.100) filled to the top. The tubes were oriented horizontally and incubated at 37 °C with shaking at 100 rpm. For the aerobic and anaerobic starvation conditions, the samples were taken after 2 h of incubation. For aerobic and anaerobic conditions that permitted growth, samples were taken during exponential growth phase. Samples were processed and analysed using mass spectrometry as described below.

Sample processing for mass spectrometry-based metabolomics. To measure metabolites in whole colonies over time, filter membranes that carried colonies were transferred into 150 µL of a mixture of 40:40:20 (v/v) acetonitrile:methanol:water at -20 °C for metabolite extraction. This suspension was vortexed with a glass bead to disrupt the colonies.

To measure extracellular metabolites from colonies, the filter membranes carrying the colonies were resuspended in 1 mL phosphate-buffered saline (PBS; 8 g l^{-1} NaCl, 0.2 g l^{-1} KCl, 1.44 g l^{-1} Na_2HPO_4, 0.24 g l^{-1} KH_2PO_4, pH 7.4) at 37 °C. In this case, no vortexing was needed, as the colonies readily dissolved. The suspension was immediately vacuum-filtered using a 0.45 µm pore size filter (HVLP02500, Merck Millipore) and 100 µL of the flow-through were mixed with 400 µL of a mixture of 50:50 (v/v) acetonitrile:methanol at -20 °C.

To measure extracellular metabolites from liquid cultures, 1 mL of grown cultures were filtered on a 0.45 µm pore size filter (HVLP02500, Merck Millipore) and 100 µL of the flow through were mixed with 400 µL of a mixture of 50:50 (v/v) acetonitrile:methanol at -20 °C.

All extracts were centrifuged for 15 minutes at 11,000 g at -9 °C and stored at -80 °C until mass spectrometry analysis.

Mass spectrometry measurements. For metabolomics, centrifuged extracts were mixed with ^{13}C-labeled internal standards. Chromatographic separation was performed on an Agilent 1290 Infinity II LC System (Agilent Technologies) equipped with an Acquity UPLC BEH Amide column (2.1 x 30 mm, particle size 1.8 µm, Waters) for acidic conditions and an iHilic-Fusion (P) HPLC column (2.1 x 50 mm, particle size 5 µm, Hilicon) for basic conditions. The following binary gradients with a flow rate of 400 µl min^{-1} were applied. Acidic condition: 0-1.3 min isocratic 10% A (water with 0.1% v/v formic acid, 10 mM ammonium formate), 90% B (acetonitrile with 0.1% v/v formic acid,),1.3-1.5 min linear from 90% to 40% B; 1.5-1.7 min linear from 40% to 90% B, 1.7-2 min isocratic 90% B. Basic condition: 0-1.3 min isocratic 10% A (water with formic acid 0.2% (v/v), 10 mM ammonium carbonate), 90% B (acetonitrile); 1.3-1.5 min linear from 90% to 40% B; 1.5-1.7 min linear from 40% to 90% B, 1.7-2 min isocratic 90% B. The injection volume was 3.0 µl (full loop injection).

Ions were detected using an Agilent 6495 triple quadrupole mass spectrometer (Agilent Technologies) equipped with an Agilent Jet Stream electrospray ion source in positive and negative ion mode. The source gas temperature was set to 200 °C, with 14 L min^{-1} drying gas and a nebulizer pressure of 24 psi. Sheath gas temperature was set to 300 °C and the flow to 11 L min^{-1}. Electrospray nozzle and capillary voltages were set to 500 and 2500 V, respectively. Metabolites were identified by multiple reaction monitoring (MRM). MRM parameters were optimized and validated with authentic standards (47). Metabolites were measured in ^{12}C and ^{13}C isoforms, and the data was analysed with a published Matlab code (47).

Data analysis for metabolomics. For whole-colony metabolite measurements, the mass spectrometry measurements were normalized by the total biovolume measured with confocal microscopy. For measurements of the extracellular metabolites in colonies (Fig. 3b), the mass spectrometry measurements were normalized by colony number and average colony volume determined by confocal microscopy. To create heatmaps of the metabolite dynamics, the Genesis software (48) was used.

Whole-colony transcriptomes. Colonies were grown on filter membranes as described above. After 12 h, 18 h, 24 h, 32 h, 42 h, 48 h, 60 h, and 72 h of growth, filters carrying the colonies were picked up using forceps and transferred into 1.5 mL Eppendorf tubes, which were immediately placed into liquid nitrogen, followed by storage at -80 °C until further processing. To extract the RNA, a glass bead and 600 µL of cell lysis buffer were added during thawing of the sample at room temperature. Cell lysis buffer consisted of TE (10 mM Tris, adjusted to pH 8.0 with HCl, 1 mM EDTA) and 1 mg/mL of chicken egg lysozyme (Sigma, L6876). The colonies were disrupted by vortexing and the cell suspension was moved to a new 1.5 mL Eppendorf tube. Then, total RNA was extracted using the hot SDS/phenol

bioRxiv preprint doi: https://doi.org/10.1101/2021.02.28.433255; this version posted February 28, 2021. The copyright holder for this preprint (which was not certified by peer review) is the author/funder, who has granted bioRxiv a license to display the preprint in perpetuity. It is made available under aCC-BY-NC-ND 4.0 International license.

method (49) with some modifications as follows. Cells were lysed at 65 °C for 2 min in the presence of 1% (w/v) SDS, and the lysate was incubated with 750 µL of Roti-Aqua-Phenol (Carl Roth, A980) at 65 °C for 8 min, followed by the addition of 750 µL chloroform (Sigma, C2432) to the aqueous phase and centrifugation using a phase lock gel tube (VWR, 733-2478). RNA was purified from this suspension by ethanol precipitation and dissolved in 60 µL of RNase-free water. Samples were then treated with TURBO DNase (Thermo Fisher, AM2238) and rRNA depletion was performed using Ribo-Zero rRNA Removal Kit for bacteria (Illumina, MRZB12424). Sequencing library preparation was carried out using NEBNext Ultra II Directional RNA Library Prep with Sample Purification Beads (NEB, E7765S). Sequencing was carried out at the Max Planck Genome Centre (Cologne, Germany) using an Illumina HiSeq3000 with 150 bp single reads. All transcriptomic analyses were performed using the software CLC Genomics Workbench v11.0 (Qiagen). The *E. coli* K-12 W3310 genome (50), parental strain of *E. coli* AR3110 (43), was used as reference for annotation. For creating heatmaps, clustering of transcripts was performed using the software Genesis (48).

Spatial transcriptomes. Filter membranes carrying colonies that were grown for 72 h were transferred into 2 mL Eppendorf tubes (one filter per tube). Cells from the colonies on a filter were then quickly suspended in 1 mL PBS by vortexing and pipetting, followed by removal of the filter from the tube, and fixation of the cells by adding formaldehyde (Sigma, F8775) to a final concentration of 4 %, for 10 min at room temperature. Formaldehyde fixation did not affect the transcriptomic profile or the fluorescence intensity (SI Appendix, Fig. S13). Then, the fixed cells were washed three times with PBS and the cell suspension was filtered with a 5 µm pore size filter (Sartorius, 17594) to remove aggregates. Cells were separated using fluorescence-activated cell sorting (BD FACSAria Fusion), using the mRuby2 fluorescence as a signal. After sorting, approximately 10^6 cells were collected in 10 mL of PBS for each bin. To concentrate the samples, they were vacuum-filtered using a 0.45 µm membrane filter (Millipore, HVLP02500). The filters containing the cells were suspended in 400 µL of the cell lysis buffer (same composition as above). The suspension was frozen in liquid nitrogen and stored at -80 °C until RNA extraction.

Total RNA was extracted using the same protocol as described above (based on the hot SDS/phenol method), but with the following modifications to minimize the number of steps and loss of RNA: after treatment with phenol, the aqueous and organic phases were both directly transferred to a phase lock gel tube (VWR, 733-2478) without centrifugation. Chloroform was added and centrifuged at 15,000 rpm for 15 min at 12 °C. After centrifugation, RNA in the aqueous phase was purified and collected in 10 µL of RNase-free water using Agencourt RNAClean XP (Beckman Coulter, A63987) according to the manufacturer's recommendations. Samples were then treated with TURBO DNase (Thermo Fisher, AM2238) and rRNA depletion was performed using Ribo-Zero rRNA Removal Kit for bacteria (Illumina, MRZB12424). Library preparation was carried out using NEBNext Ultra II Directional RNA Library Prep with Sample Purification Beads (NEB, E7765S). Sequencing was carried out at the Max Planck Genome Centre (Cologne, Germany) using an Illumina HiSeq3000 with 150 bp single reads.

Measurements of the fraction of dead cells. To measure the fraction of dead cells within the aerobic region of the colonies, the colonies were grown on filter membranes on M9 agar as described above, but with the exception that SYTOX Green (Thermofisher, S7020) with a final concentration of 2.5 µM was added to the M9 agar plates. SYTOX Green is a nucleic acid stain that can only diffuse into dead cells with a compromised cell membrane. After incubation for 72 h, the mRuby2 fluorescence and the SYTOX Green fluorescence in the colonies was imaged using confocal microscopy. Inside the colony, 3D regions that were fluorescent in both the mRuby2 and SYTOX Green channels were identified *via* thresholding. The fraction of dead cells was calculated as the thresholded volume present in both the mRuby2 and SYTOX Green channels, divided by the thresholded volume of the mRuby2 channel. For the quantification of the fraction of dead cells in the aerobic region of the colony, only cells located within 30 µm from the outer surface of the colony were considered, because only in this region oxygen penetration was high enough to generate a sufficiently strong mRuby2 signal.

To measure the fraction of dead cells in liquid cultures, cultures were grown in M9 medium, which was supplemented with SYTOX Green (2.5 µM), incubated at 37 °C inside 96-well plates with continuous shaking. The OD_{600} and SYTOX Green fluorescence were measured in a microtiter plater reader (Spark 10M, Tecan). The fraction of dead cells was calculated as the SYTOX Green fluorescence normalized by the OD_{600}.

Oxygen measurements. Oxygen concentrations were measured in 72-h-old colonies (grown on M9 agar as described above) using a 25-µm-tip oxygen microsensor (Unisense OX-25) according to the

bioRxiv preprint doi: https://doi.org/10.1101/2021.02.28.433255; this version posted February 28, 2021. The copyright holder for this preprint (which was not certified by peer review) is the author/funder, who has granted bioRxiv a license to display the preprint in perpetuity. It is made available under aCC-BY-NC-ND 4.0 International license.

manufacturer's instructions. Briefly, the oxygen microsensor was calibrated using a two-point calibration. The microsensor was first calibrated to atmospheric oxygen using a calibration chamber (Unisense CAL300) containing water continuously bubbled with air. The microsensor was then calibrated to a "zero" oxygen point using an anoxic solution of 0.1 M sodium ascorbate and 0.1 M sodium hydroxide in water. Oxygen measurements were then taken through the top ≥100 µm of the colony biofilm in 5-µm-steps using a measurement time of 3 s at each position, and a wait time between measurements of 5 s. A micromanipulator (Unisense MM33) was used to move the microsensor within the colony. Profiles were recorded using a multimeter (Unisense) and the SensorTrace Profiling software (Unisense).

Statistical analysis. Statistical analysis was carried out using GraphPad Prism v8 (GraphPad Software), except for the statistical analysis for transcriptomic data, which was performed using the software CLC Genomics Workbench 11.0 (Qiagen).

References

1. H.-C. Flemming, *et al.*, Biofilms: an emergent form of bacterial life. *Nat. Rev. Microbiol.* **14**, 563–575 (2016).
2. H.-C. Flemming, S. Wuertz, Bacteria and archaea on Earth and their abundance in biofilms. *Nat. Rev. Microbiol.* **17**, 247–260 (2019).
3. M. Ackermann, A functional perspective on phenotypic heterogeneity in microorganisms. *Nat. Rev. Microbiol.* **13**, 497–508 (2015).
4. C. R. Evans, C. P. Kempes, A. Price-Whelan, L. E. P. Dietrich, Metabolic Heterogeneity and Cross-Feeding in Bacterial Multicellular Systems. *Trends Microbiol.* **28**, 732–743 (2020).
5. P. S. Stewart, M. J. Franklin, Physiological heterogeneity in biofilms. *Nat. Rev. Microbiol.* **6**, 199–210 (2008).
6. M. San Roman, A. Wagner, An enormous potential for niche construction through bacterial cross-feeding in a homogeneous environment. *PLOS Comput. Biol.* **14**, e1006340 (2018).
7. N. W. Smith, P. R. Shorten, E. Altermann, N. C. Roy, W. C. McNabb, The Classification and Evolution of Bacterial Cross-Feeding. *Front. Ecol. Evol.* **7**, 1–15 (2019).
8. K. T. Schiessl, *et al.*, Phenazine production promotes antibiotic tolerance and metabolic heterogeneity in Pseudomonas aeruginosa biofilms. *Nat. Commun.* **10**, 762 (2019).
9. S. H. Saunders, *et al.*, Extracellular DNA Promotes Efficient Extracellular Electron Transfer by Pyocyanin in Pseudomonas aeruginosa Biofilms. *Cell* **182**, 919-932.e19 (2020).
10. J. M. Flynn, D. Niccum, J. M. Dunitz, R. C. Hunter, Evidence and Role for Bacterial Mucin Degradation in Cystic Fibrosis Airway Disease. *PLoS Pathog.* **12**, e1005846 (2016).
11. C. M. Prieto-Barajas, E. Valencia-Cantero, G. Santoyo, Microbial mat ecosystems: Structure types, functional diversity, and biotechnological application. *Electron. J. Biotechnol.* **31**, 48–56 (2018).
12. Y. Lin, *et al.*, Phenazines Regulate Nap-Dependent Denitrification in Pseudomonas aeruginosa Biofilms. *J. Bacteriol.* **200**, 1–17 (2018).
13. A. Z. Rosenthal, *et al.*, Metabolic interactions between dynamic bacterial subpopulations. *Elife* **7**, 1–18 (2018).
14. N. Nikolic, *et al.*, Cell-to-cell variation and specialization in sugar metabolism in clonal bacterial populations. *PLoS Genet.* **13**, 1–24 (2017).
15. M. Kinnersley, *et al.*, Ex Uno Plures: Clonal Reinforcement Drives Evolution of a Simple Microbial Community. *PLoS Genet.* **10**, e1004430 (2014).
16. Y.-L. Yang, Y. Xu, P. Straight, P. C. Dorrestein, Translating metabolic exchange with imaging mass spectrometry. *Nat. Chem. Biol.* **5**, 885–887 (2009).
17. J. D. Watrous, *et al.*, Microbial metabolic exchange in 3D. *ISME J.* **7**, 770–780 (2013).
18. W. J. Moree, *et al.*, Interkingdom metabolic transformations captured by microbial imaging mass spectrometry. *Proc. Natl. Acad. Sci.* **109**, 13811–13816 (2012).
19. D. Kim, *et al.*, Candida albicans stimulates Streptococcus mutans microcolony development via cross-kingdom biofilm-derived metabolites. *Sci. Rep.* **7**, 41332 (2017).
20. M. A. Henson, G. Orazi, P. Phalak, G. A. O'Toole, Metabolic Modeling of Cystic Fibrosis Airway Communities Predicts Mechanisms of Pathogen Dominance. *mSystems* **4**, 1–20 (2019).
21. S. Pande, *et al.*, Privatization of cooperative benefits stabilizes mutualistic cross-feeding interactions in spatially structured environments. *ISME J.* **10**, 1413–1423 (2016).
22. J. Liu, *et al.*, Metabolic co-dependence gives rise to collective oscillations within biofilms. *Nature* **523**, 550–554 (2015).

bioRxiv preprint doi: https://doi.org/10.1101/2021.02.28.433255; this version posted February 28, 2021. The copyright holder for this preprint (which was not certified by peer review) is the author/funder, who has granted bioRxiv a license to display the preprint in perpetuity. It is made available under aCC-BY-NC-ND 4.0 International license.

23. J. A. Cole, L. Kohler, J. Hedhli, Z. Luthey-Schulten, Spatially-resolved metabolic cooperativity within dense bacterial colonies. *BMC Syst. Biol.* **9**, 15 (2015).
24. E. Wolfsberg, C. P. Long, M. R. Antoniewicz, Metabolism in dense microbial colonies: 13C metabolic flux analysis of E. coli grown on agar identifies two distinct cell populations with acetate cross-feeding. *Metab. Eng.* **49**, 242–247 (2018).
25. A. Dal Co, S. van Vliet, M. Ackermann, Emergent microscale gradients give rise to metabolic cross-feeding and antibiotic tolerance in clonal bacterial populations. *Philos. Trans. R. Soc. Lond. B. Biol. Sci.* **374**, 20190080 (2019).
26. Y. Lin, W. C. Cornell, J. Jo, A. Price-Whelan, L. E. P. Dietrich, The Pseudomonas aeruginosa Complement of Lactate Dehydrogenases Enables Use of D- and L-Lactate and Metabolic Cross-Feeding. *MBio* **9**, 1–12 (2018).
27. E. Bauer, J. Zimmermann, F. Baldini, I. Thiele, C. Kaleta, BacArena : Individual-based metabolic modeling of heterogeneous microbes in complex communities. 1–22 (2017).
28. C. Liao, T. Wang, S. Maslov, J. B. Xavier, Modeling microbial cross-feeding at intermediate scale portrays community dynamics and species coexistence. *PLoS Comput. Biol.* **16**, e1008135 (2020).
29. R. Y. Tsien, The green fluorescent protein. *Annu. Rev. Biochem.* **67**, 509–44 (1998).
30. M. R. Warren, *et al.*, Spatiotemporal establishment of dense bacterial colonies growing on hard agar. *Elife* **8**, 1–47 (2019).
31. S. J. Pirt, A kinetic study of the mode of growth of surface colonies of bacteria and fungi. *J. Gen. Microbiol.* **47**, 181–97 (1967).
32. M. San Roman, A. Wagner, Acetate and glycerol are not uniquely suited for the evolution of cross-feeding in E. coli. *PLOS Comput. Biol.* **16**, e1008433 (2020).
33. H. Hori, *et al.*, Inducible L-alanine exporter encoded by the novel gene ygaW (alaE) in Escherichia coli. *Appl. Environ. Microbiol.* **77**, 4027–34 (2011).
34. A. J. Lam, *et al.*, Improving FRET dynamic range with bright green and red fluorescent proteins. *Nat. Methods* **9**, 1005–12 (2012).
35. J. Jo, K. L. Cortez, W. C. Cornell, A. Price-Whelan, L. E. P. Dietrich, An orphan cbb3-type cytochrome oxidase subunit supports Pseudomonas aeruginosa biofilm growth and virulence. *Elife* **6**, 1–30 (2017).
36. M. Lobocka, J. Hennig, J. Wild, T. Kłopotowski, Organization and expression of the Escherichia coli K-12 dad operon encoding the smaller subunit of D-amino acid dehydrogenase and the catabolic alanine racemase. *J. Bacteriol.* **176**, 1500–10 (1994).
37. S. Katsube, K. Sato, T. Ando, E. Isogai, H. Yoneyama, Secretion of d-alanine by Escherichia coli. *Microbiology* **162**, 1243–1252 (2016).
38. S. Katsube, T. Ando, H. Yoneyama, L-Alanine Exporter, AlaE, of Escherichia coli Functions as a Safety Valve to Enhance Survival under Feast Conditions. *Int. J. Mol. Sci.* **20**, 4942 (2019).
39. J. B. Andersen, *et al.*, New unstable variants of green fluorescent protein for studies of transient gene expression in bacteria. *Appl. Environ. Microbiol.* **64**, 2240–2246 (1998).
40. M. Basan, *et al.*, Overflow metabolism in Escherichia coli results from efficient proteome allocation. *Nature* **528**, 99–104 (2015).
41. H. Tsuchiya, *et al.*, Structural basis for amino acid export by DMT superfamily transporter YddG. *Nature* **534**, 417–20 (2016).
42. I. Franke, A. Resch, T. Dassler, T. Maier, A. Bock, YfiK from Escherichia coli Promotes Export of O-Acetylserine and Cysteine. *J. Bacteriol.* **185**, 1161–1166 (2003).
43. D. O. Serra, A. M. Richter, R. Hengge, Cellulose as an Architectural Element in Spatially Structured Escherichia coli Biofilms. *J. Bacteriol.* **195**, 5540–5554 (2013).
44. J. Sambrook, E. . Fritsch, T. Maniatis, *Molecular Cloning: a laboratory manual*, 2nd Ed. (Cold Spring Harbor Laboratory Press, 1989).
45. K.-H. Choi, *et al.*, A Tn7-based broad-range bacterial cloning and expression system. *Nat. Methods* **2**, 443–448 (2005).
46. H. Jeckel, K. Drescher, Advances and opportunities in image analysis of bacterial cells and communities. *FEMS Microbiol. Rev.*, 1–14 (2020).
47. J. C. Guder, T. Schramm, T. Sander, H. Link, Time-Optimized Isotope Ratio LC–MS/MS for High-Throughput Quantification of Primary Metabolites. *Anal. Chem.* **89**, 1624–1631 (2017).
48. A. Sturn, J. Quackenbush, Z. Trajanoski, Genesis: cluster analysis of microarray data. *Bioinformatics* **18**, 207–8 (2002).
49. C. E. Jahn, A. O. Charkowski, D. K. Willis, Evaluation of isolation methods and RNA integrity for bacterial RNA quantitation. *J. Microbiol. Methods* **75**, 318–24 (2008).
50. K. Hayashi, *et al.*, Highly accurate genome sequences of Escherichia coli K-12 strains

bioRxiv preprint doi: https://doi.org/10.1101/2021.02.28.433255; this version posted February 28, 2021. The copyright holder for this preprint (which was not certified by peer review) is the author/funder, who has granted bioRxiv a license to display the preprint in perpetuity. It is made available under aCC-BY-NC-ND 4.0 International license.

MG1655 and W3110. *Mol. Syst. Biol.* **2** (2006).

51. L. Hobley, C. Harkins, C. E. MacPhee, N. R. Stanley-Wall, Giving structure to the biofilm matrix: an overview of individual strategies and emerging common themes. *FEMS Microbiol. Rev.* **39**, 649–669 (2015).
52. L. Vidakovic, P. K. Singh, R. Hartmann, C. D. Nadell, K. Drescher, Dynamic biofilm architecture confers individual and collective mechanisms of viral protection. *Nat. Microbiol.* **3**, 26–31 (2018).
53. K. A. Datsenko, B. L. Wanner, One-step inactivation of chromosomal genes in Escherichia coli K-12 using PCR products. *Proc. Natl. Acad. Sci. U. S. A.* **97**, 6640–5 (2000).
54. P. P. Cherepanov, W. Wackernagel, Gene disruption in Escherichia coli: TcR and KmR cassettes with the option of Flp-catalyzed excision of the antibiotic-resistance determinant. *Gene* **158**, 9–14 (1995).

bioRxiv preprint doi: https://doi.org/10.1101/2021.02.28.433255; this version posted February 28, 2021. The copyright holder for this preprint (which was not certified by peer review) is the author/funder, who has granted bioRxiv a license to display the preprint in perpetuity. It is made available under aCC-BY-NC-ND 4.0 International license.

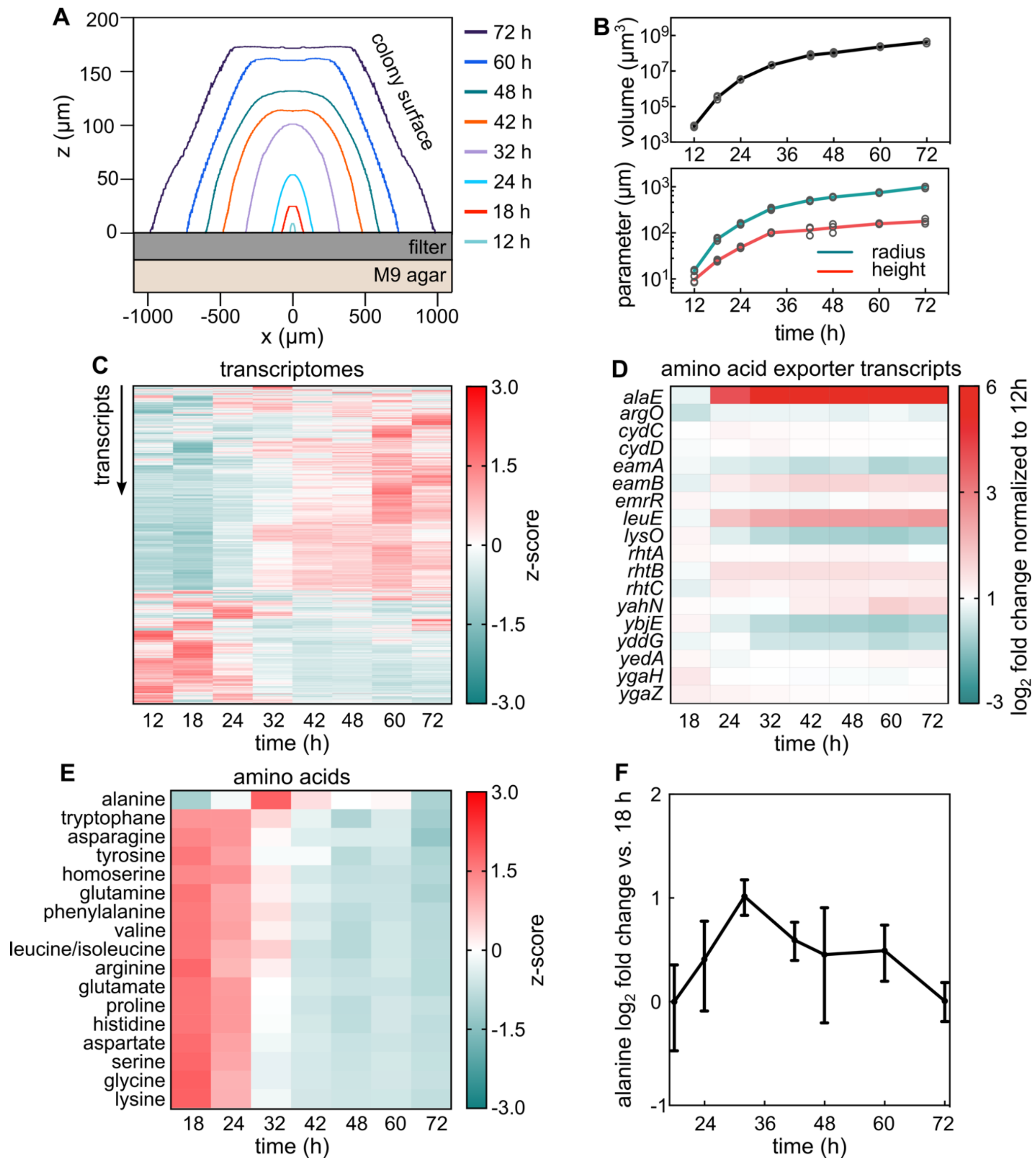

Figure 1. Transcriptomes and metabolomes during *E. coli* colony biofilm growth reveal metabolic transition and a special role of alanine. (*A*) Cross-sectional profile of *E. coli* colonies grown on membrane filters placed on solid M9 agar at different time points. Each line corresponds to the surface of a representative colony. (*B*) Volume (top panel), radius and height (bottom panel) of colonies as a function of time indicate a growth rate transition around 24-32 h. All replicates are shown as individual data points, with a line connecting the mean values, $n = 3$. (*C*) Dynamics of expression profiles of 4,231 genes during colony growth reveal physiological transition between 24-32 h, $n = 3$. (*D*) Mean expression fold-changes of known amino acid exporters during colony growth, calculated in comparison to 12 h colonies, $n = 3$. (*E*) Amino acid dynamics measured from whole colonies during colony growth, $n = 3$. (*F*) Fold-change of alanine levels inside whole colonies, calculated in comparison to 18 h colonies. Data are mean ± s.d., $n = 3$.

bioRxiv preprint doi: https://doi.org/10.1101/2021.02.28.433255; this version posted February 28, 2021. The copyright holder for this preprint (which was not certified by peer review) is the author/funder, who has granted bioRxiv a license to display the preprint in perpetuity. It is made available under aCC-BY-NC-ND 4.0 International license.

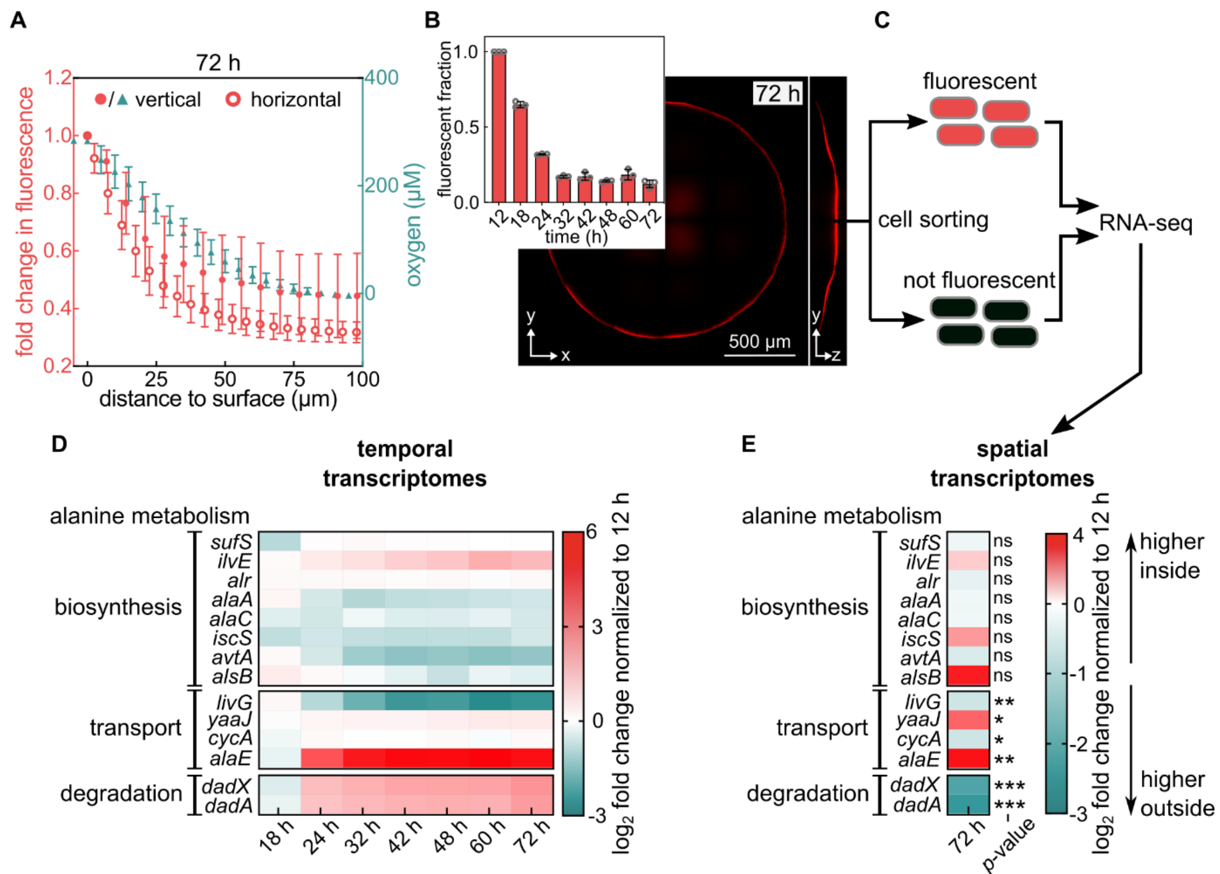

Figure 2. Alanine transport and degradation are spatially regulated within colony biofilms. (*A*) Measurement of oxygen penetration into colonies grown for 72 h on filter membranes on M9 agar using two different methods (for strain KDE722). Left axis (red): Intensity of mRuby2 fluorescence within a vertical cylinder of radius 3.3 μm in the center of the colony (filled circles), and intensity of mRuby2 fluorescence within a horizontal plane at the base of the colony (open circles, mean ± s.d., $n = 3$). Right axis (green): Direct measurement of oxygen levels acquired by vertical scanning of an oxygen microsensor at the center of the colony (green triangles, mean ± s.d., $n = 10$). (*B*) Confocal image of a representative 72 h colony of a strain that constitutively expresses mRuby2 (KDE722). Insert: Fraction of fluorescent biovolume inside colonies grown for different times. Data are mean ± s.d., $n = 3$. (*C*) Scheme of the sorting procedure: Cells from a 72 h colony are separated, fixed using formaldehyde, and sorted according to their mRuby2 fluorescence, followed by RNA-seq, as described in the methods section. (*D*) Heatmaps showing the mean fold-change ($n = 3$) of expression levels of genes involved in alanine metabolism, from whole-colony measurements. Fold-changes are computed relative to the 12 h timepoint. (*E*) Spatial transcriptome results, quantified as fold-changes between the inner region (no mRuby2 fluorescence) and outer region (high mRuby2 fluorescence) regions of colonies grown for 72 h. Red color in the heatmap indicates genes with higher transcript levels in the inner region of the colony, green color indicates higher transcripts in the outer region of the colony. Data are means, $n = 4$. Non-significant differences between spatial regions are labelled "ns". *p*-values correspond to false discovery rate (FDR)-adjusted *p*-values: * $p < 0.05$, ** $p < 0.01$, *** $p < 0.001$.

bioRxiv preprint doi: https://doi.org/10.1101/2021.02.28.433255; this version posted February 28, 2021. The copyright holder for this preprint (which was not certified by peer review) is the author/funder, who has granted bioRxiv a license to display the preprint in perpetuity. It is made available under aCC-BY-NC-ND 4.0 International license.

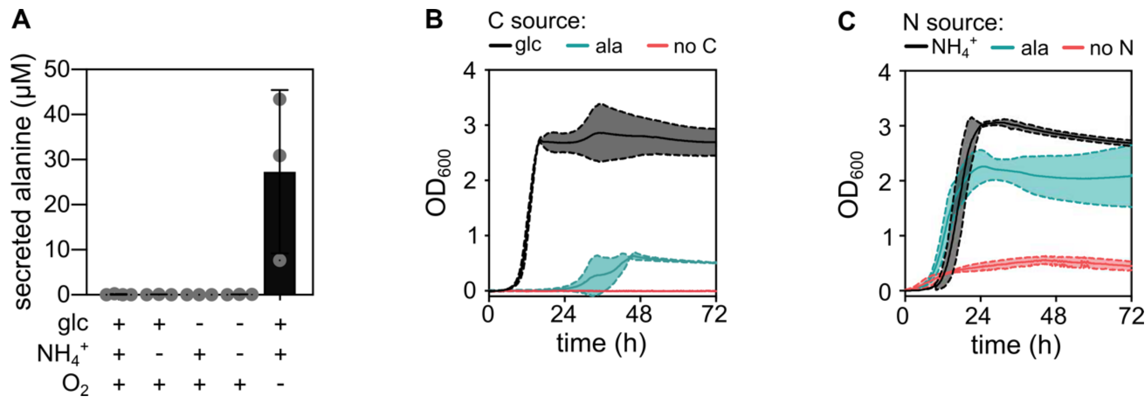

Figure 3. Alanine can be secreted and consumed by *E. coli.* (*A*) Extracellular alanine concentration in the supernatant of liquid cultures grown in presence or absence (indicated by + or -) of glucose (glc), ammonium (NH_4^+), and molecular oxygen (O_2). (*B*) Growth curves using M9 minimal salts medium with ammonium as nitrogen source and different carbon (C) sources: Either glucose (5 g/L, as in our standard M9 medium), alanine (10 mM), or no carbon source. (*C*) Growth curves using M9 minimal salts medium with glucose as a carbon source and different nitrogen (N) sources: Either ammonium (22.6 mM, as in our standard M9 medium), alanine (5 mM) or no nitrogen source. For panels *B* and *C*, continuous middle lines correspond to the mean and the dotted lines to the standard deviation, $n = 3$. The growth curves shown for alanine in panels *B* and *C* correspond to the alanine concentrations that resulted in the highest final OD_{600} in each condition.

bioRxiv preprint doi: https://doi.org/10.1101/2021.02.28.433255; this version posted February 28, 2021. The copyright holder for this preprint (which was not certified by peer review) is the author/funder, who has granted bioRxiv a license to display the preprint in perpetuity. It is made available under aCC-BY-NC-ND 4.0 International license.

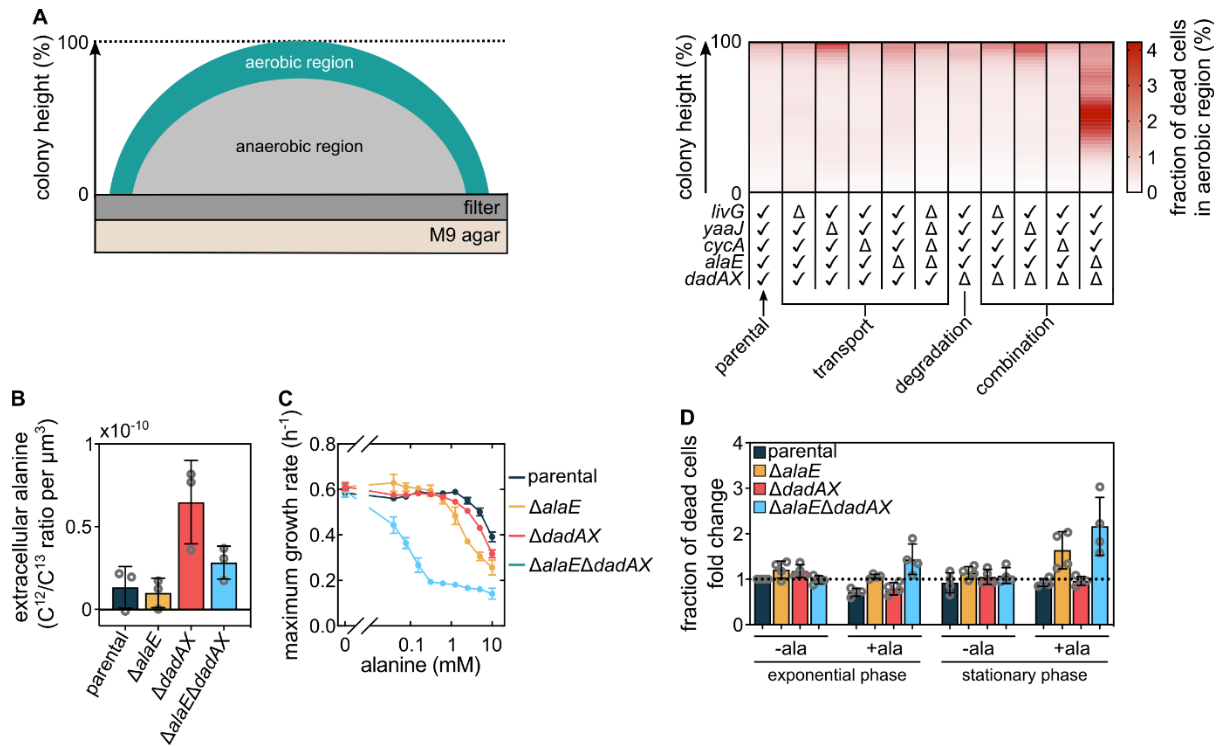

Figure 4. Alanine influences cell viability and growth. (*A*) Measurement of the fraction of dead cells as a function of height in colonies grown for 72 h on M9 agar. These measurements were performed only for cells located within 30 µm from the outer colony surface, which is a conservative measurement of the aerobic region (Fig. 2A). The table designates the genotype of strains that were investigated: "✓" indicates that the gene is intact and "Δ" that the gene was deleted. Data in the heatmaps shows means, $n = 3$. Errors are shown in the SI Appendix, Fig. S10. (*B*) Extracellular alanine levels measured from colonies (mean ± s.d., $n = 3$). (*C*) Maximum liquid culture growth rate (in presence of glucose and ammonium) for different strains, as a function of the concentration of exogenously added alanine. Data are mean ± s.d., $n = 3$. (*D*) Fraction of dead cells, measured using SYTOX Green fluorescence normalized by OD_{600}, in cultures grown with glucose and ammonium in presence or absence of 5 mM alanine. Fold-changes are calculated relative to the parental strain in exponential phase without alanine. Measurements were performed when cultures reached half of the maximum OD_{600} (for exponential phase measurements) or when they reached their maximum OD_{600} (for stationary phase measurements). Bars indicate mean ± s.d., $n = 4$.

bioRxiv preprint doi: https://doi.org/10.1101/2021.02.28.433255; this version posted February 28, 2021. The copyright holder for this preprint (which was not certified by peer review) is the author/funder, who has granted bioRxiv a license to display the preprint in perpetuity. It is made available under aCC-BY-NC-ND 4.0 International license.

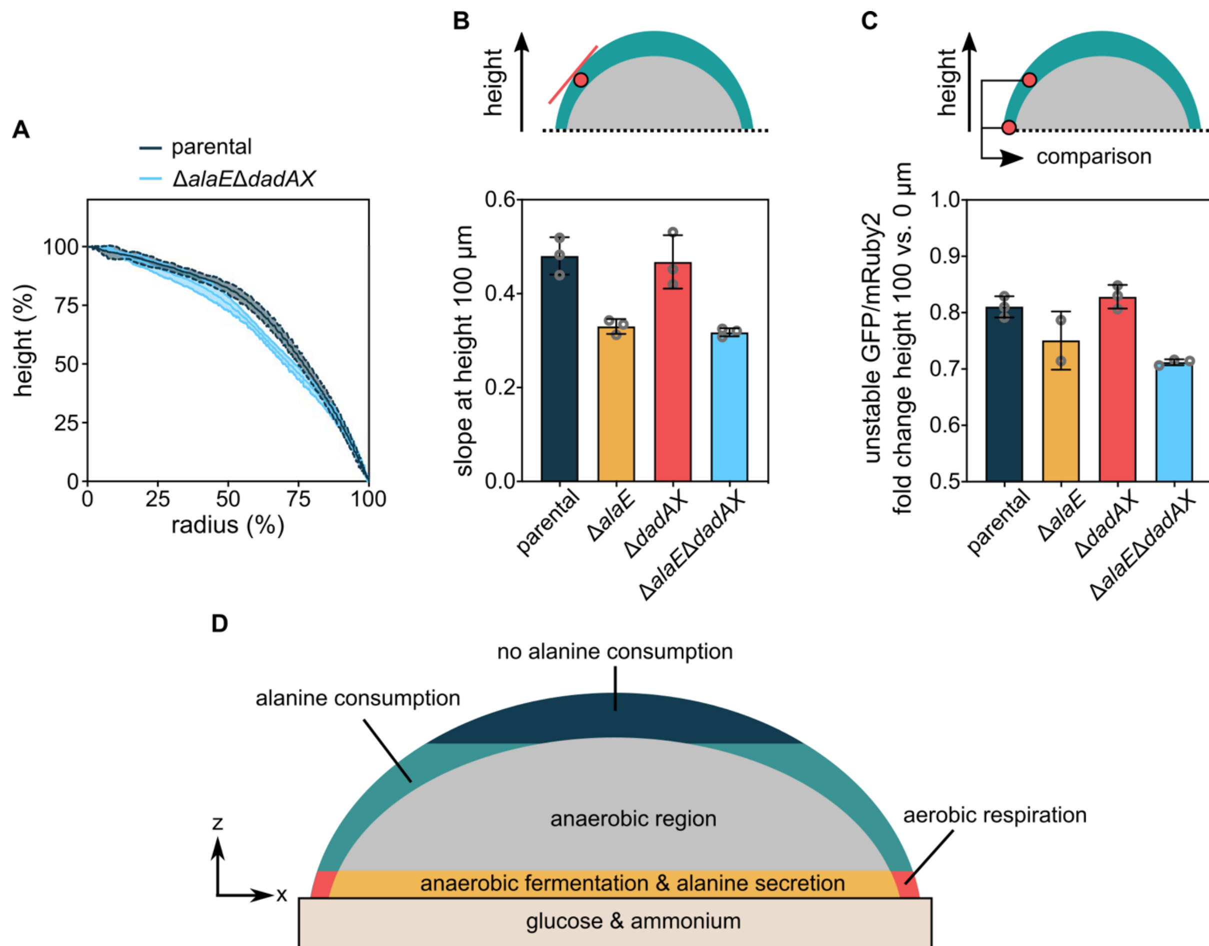

Figure 5. Colony morphology is influenced by alanine cross-feeding. (*A*) Colony height as a function of the colony radius, for colonies grown for 72 h. Central lines correspond to the mean and the shaded area to the s.d., $n = 3$. (*B*) Slope of curves in panel *A* at height 100 µm. Data are mean ± s.d., $n = 3$. (*C*) Fluorescence ratio of constitutively expressed unstable GFP and stable mRuby2, which is a measure for the cellular growth rate, as shown in the SI Appendix, Fig. S12. The unstable GFP was constructed by adding the ASV-tag to superfolder GFP. The fold-change of this fluorescent protein ratio was calculated for the aerobic colony region between the heights 100 µm and 0 µm. The fluorescent protein ratio was only measured for cells located within 30 µm from the outer colony surface, as a conservative measure of the aerobic region. Data are mean ± s.d., $n = 3$. (*D*) Model for alanine cross-feeding in *E. coli* colony biofilms grown for 72 h. Glucose and ammonium are provided in the solid M9 agar. Cells in the bottom layer of the biofilm have access to glucose and ammonium. Only cells in the outer periphery of the biofilm have access to oxygen. Cells in the red region can use ammonium, glucose, and oxygen to perform aerobic respiration. Cells in yellow region have access to glucose and ammonium, but not oxygen. These cells secrete alanine. The secreted alanine can be consumed by the aerobic cells above this layer (depicted as green), which convert alanine into pyruvate and ammonium that can be used for growth and to maintain cell viability.

bioRxiv preprint doi: https://doi.org/10.1101/2021.02.28.433255; this version posted February 28, 2021. The copyright holder for this preprint (which was not certified by peer review) is the author/funder, who has granted bioRxiv a license to display the preprint in perpetuity. It is made available under aCC-BY-NC-ND 4.0 International license.

Supplementary Information

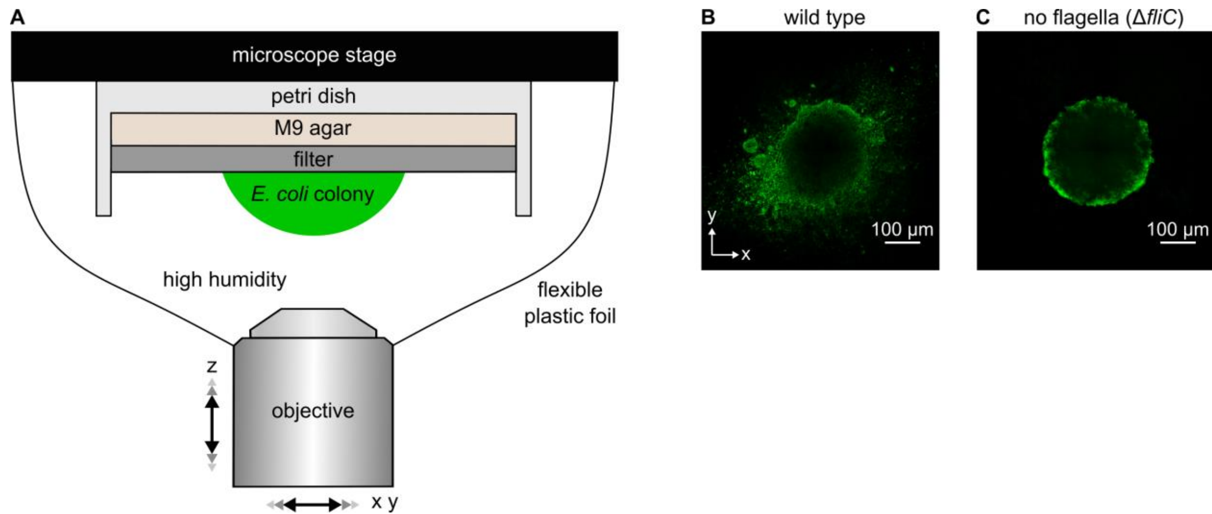

Figure S1. In contrast to wild-type colonies, flagella-deficient (Δ*fliC*) colonies are highly symmetric in shape. (*A*) Experimental arrangement for investigating colony growth using an inverted confocal microscope. Dimensions are not drawn to scale. (*B*, *C*) Confocal microscopy images of *xy*-planes of colonies on filter membranes on M9 agar, made by the wild type strain (panel *B*) or a strain lacking the flagellin gene *fliC* (panel *C*) grown for 24 h. The Δ*fliC* strain produces no flagella and is incapable of swimming motility.

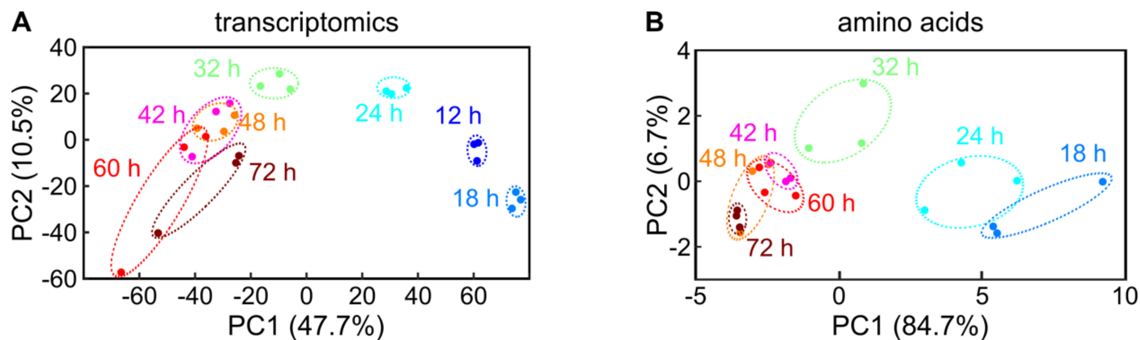

Figure S2. Principal component analysis of transcriptomic and metabolomic data. (*A*) Principal component analysis of the transcriptomic data presented in Fig. 1C. The axes represent the 1st principal component (PC1) and the 2nd principal component (PC2). (*B*) Principal component analysis of amino acid data presented in Fig. 1E. Each circle represents a different independent transcriptome or metabolome replicate. Replicates for the same colony growth timepoint have the same color and are enclosed by an ellipse with a dashed line.

bioRxiv preprint doi: https://doi.org/10.1101/2021.02.28.433255; this version posted February 28, 2021. The copyright holder for this preprint (which was not certified by peer review) is the author/funder, who has granted bioRxiv a license to display the preprint in perpetuity. It is made available under aCC-BY-NC-ND 4.0 International license.

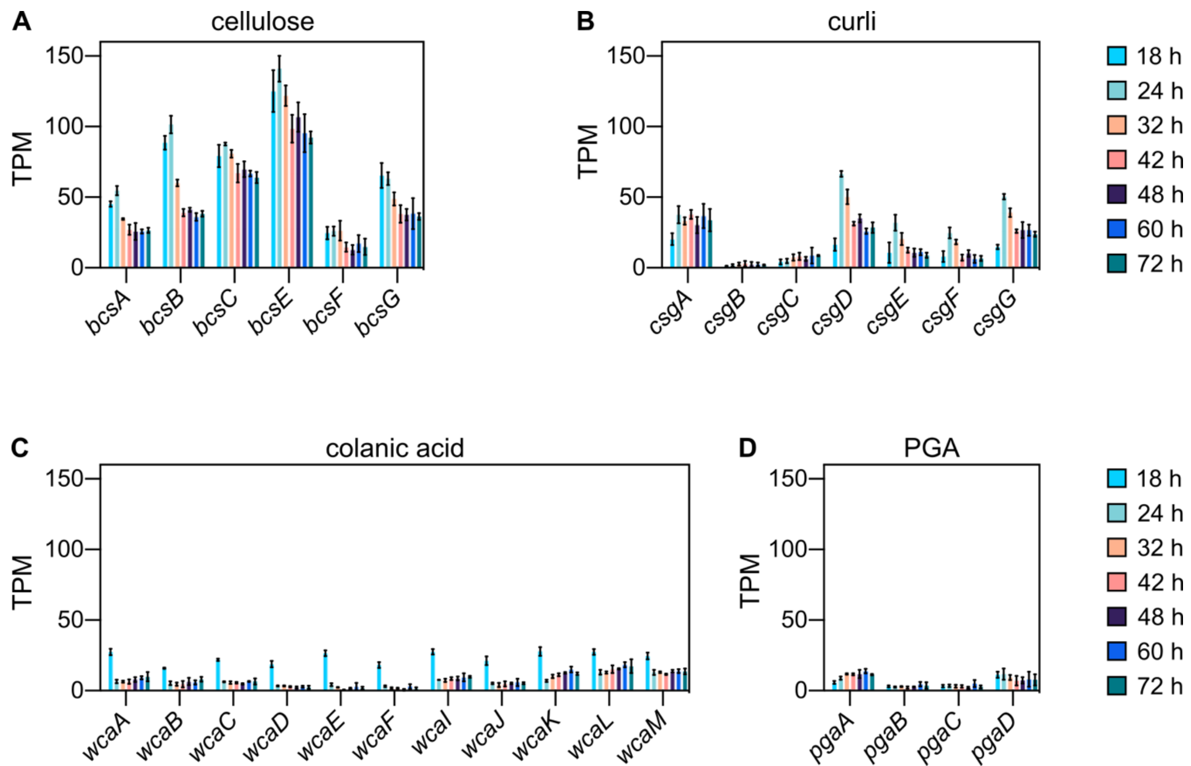

Figure S3. *E. coli* biofilm colonies express extracellular matrix genes. *E. coli* extracellular matrix is composed of cellulose, curli, colanic acid, β-1,6-N-acetyl-D-glucosamine (PGA) and flagella (51). Here, transcripts per million (TPM) of genes involved in the production of cellulose (*A*), curli (*B*), colonic acid (*C*) and PGA (*D*) are shown for colonies of the parental strain (KDE722) grown for 18 h, 24 h, 32 h, 42 h, 48 h, 60 h, or 72 h, measured using RNA-seq. Flagellar genes are not shown here, because the flagellin gene *fliC* is deleted in the parental strain. Data are mean ± standard deviation (s.d.), $n = 3$.

bioRxiv preprint doi: https://doi.org/10.1101/2021.02.28.433255; this version posted February 28, 2021. The copyright holder for this preprint (which was not certified by peer review) is the author/funder, who has granted bioRxiv a license to display the preprint in perpetuity. It is made available under aCC-BY-NC-ND 4.0 International license.

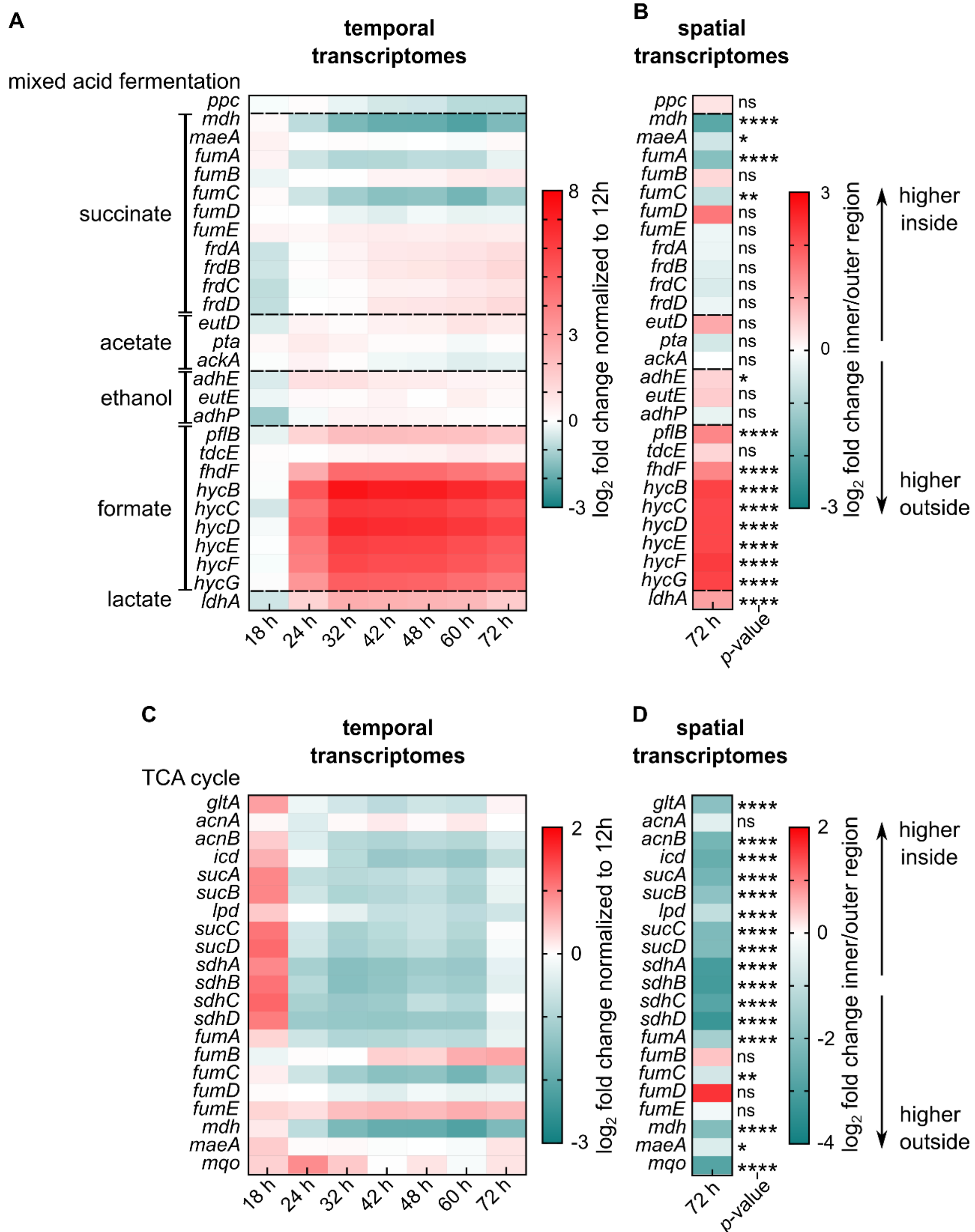

Figure S4. Spatial and temporal expression of genes involved in mixed acid fermentation and TCA cycle in colonies on M9 agar. (*A*, *B*) Heatmaps show genes involved in mixed acid fermentation. (*A*) Fold-changes of genes from whole-colony measurements at different growth stages, normalized to transcriptomes of 12 h colonies. (*B*) Fold-changes of genes from spatially-resolved transcriptomes, measured for 72 h colonies. The inner region corresponds to non-fluorescent cells, the outer region corresponds to those cells with mRuby2 fluorescence. (*C*, *D*) Heatmaps show genes involved in the TCA cycle. (*C*) Fold-changes of genes from whole-colony measurements at different growth stages, normalized to transcriptomes of 12 h colonies. (*D*) Fold-changes of genes from spatially-resolved transcriptomes, measured for 72 h colonies. Non-significant differences are labelled "ns". *p*-values correspond to FDR-adjusted *p*-values: * $p < 0.05$, ** $p < 0.01$, **** $p < 0.0001$. For panels *A* and *C*, $n = 3$; for *B* and *D*, $n = 4$. Some genes are involved in both pathways and are therefore displayed in all heatmaps.

bioRxiv preprint doi: https://doi.org/10.1101/2021.02.28.433255; this version posted February 28, 2021. The copyright holder for this preprint (which was not certified by peer review) is the author/funder, who has granted bioRxiv a license to display the preprint in perpetuity. It is made available under aCC-BY-NC-ND 4.0 International license.

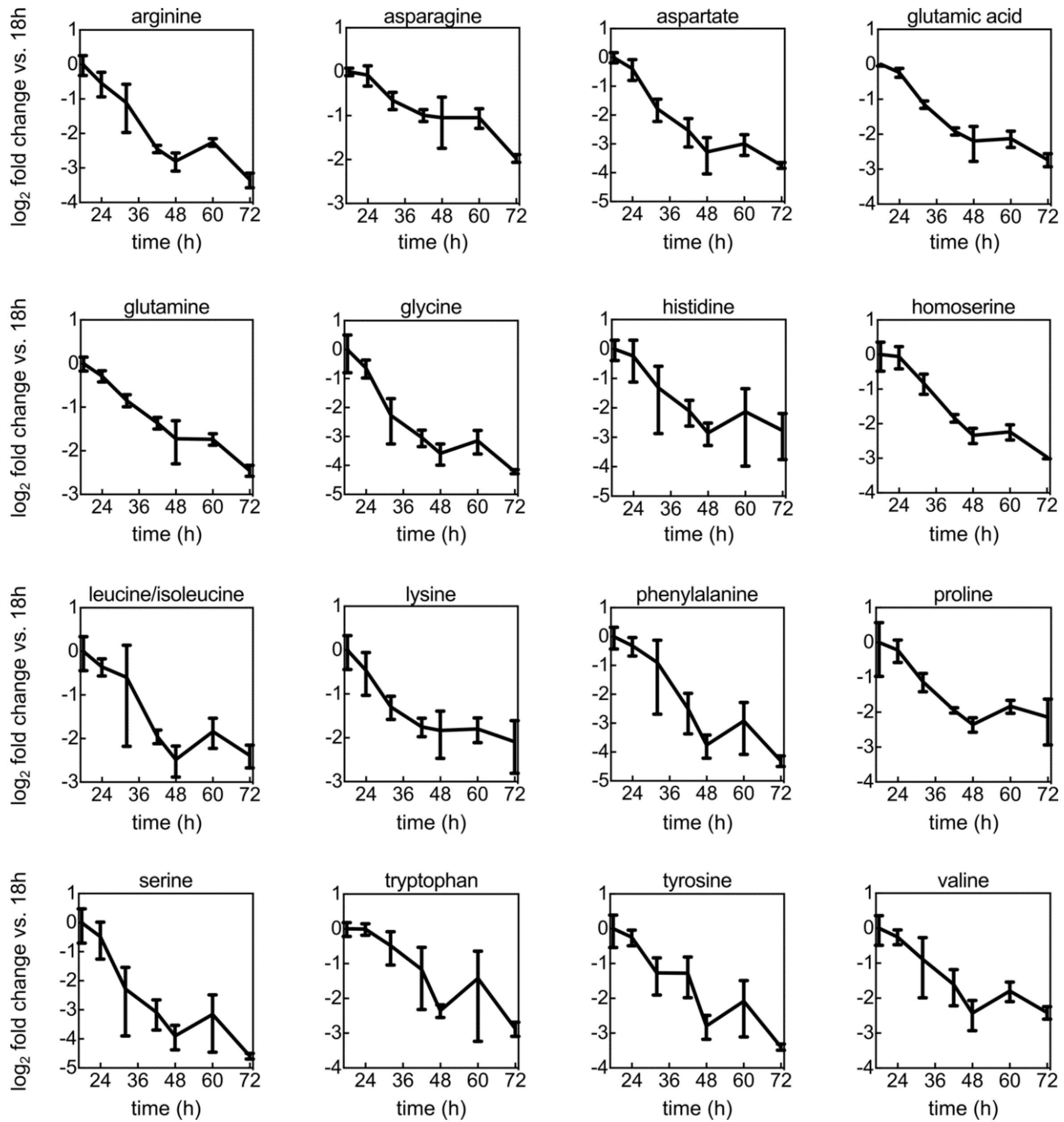

Figure S5. Amino acid levels during colony growth. Fold-changes of amino acid levels as a function of time during colony development on M9 agar, normalized to amino acid levels from 18 h colonies. Measurements were performed using mass spectrometry. Data are mean values ± s.d., $n = 3$.

bioRxiv preprint doi: https://doi.org/10.1101/2021.02.28.433255; this version posted February 28, 2021. The copyright holder for this preprint (which was not certified by peer review) is the author/funder, who has granted bioRxiv a license to display the preprint in perpetuity. It is made available under aCC-BY-NC-ND 4.0 International license.

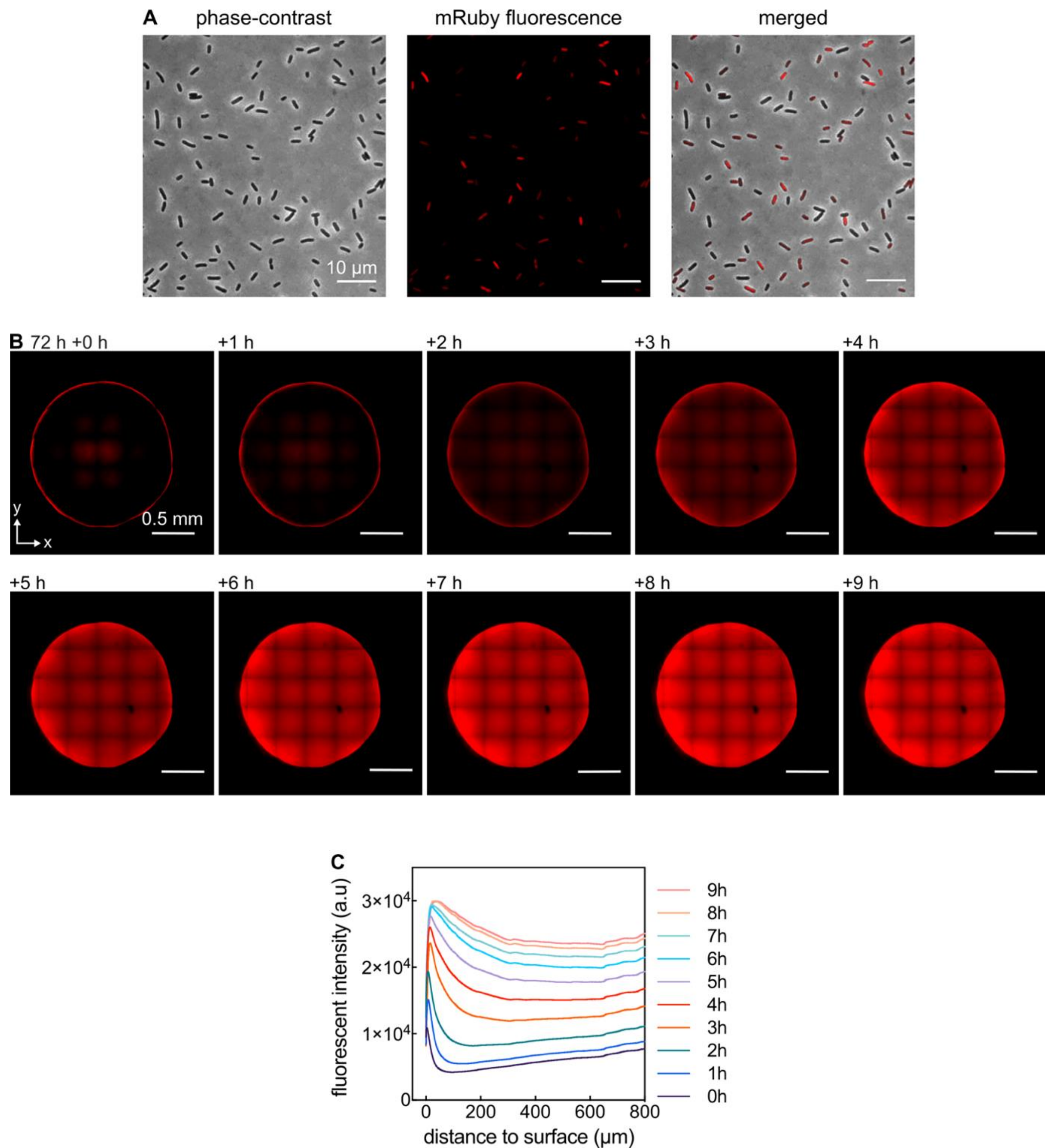

Figure S6. Fluorescent gradients of mRuby2 in colonies are not due to imaging artefacts. (*A*) Images of cells from a 72 h colony that was resuspended in PBS. Some cells are fluorescent, others display less or no fluorescence. (*B*) Confocal images of a *xy*-plane of a 72 h colony acquired at $z = 60$ µm above the filter membrane on M9 agar. At 72 h + 0 h the filter membrane carrying the colony was moved from M9 agar to an agar plate with the same medium, but lacking glucose. As a consequence, cells stop growth and stop consuming molecular oxygen, allowing oxygen to penetrate into the colony. Penetration of oxygen allows the mRuby2 protein to fold into the fluorescent conformation. The square pattern in the images results from the fact that colony images were stitched together from 7 x 7 image tiles. (*C*) Quantification of panel *B*: Fluorescent intensity for different times after transferring the colony to M9 agar without glucose (different colored lines), as a function of distance to the outer surface of the colony.

bioRxiv preprint doi: https://doi.org/10.1101/2021.02.28.433255; this version posted February 28, 2021. The copyright holder for this preprint (which was not certified by peer review) is the author/funder, who has granted bioRxiv a license to display the preprint in perpetuity. It is made available under aCC-BY-NC-ND 4.0 International license.

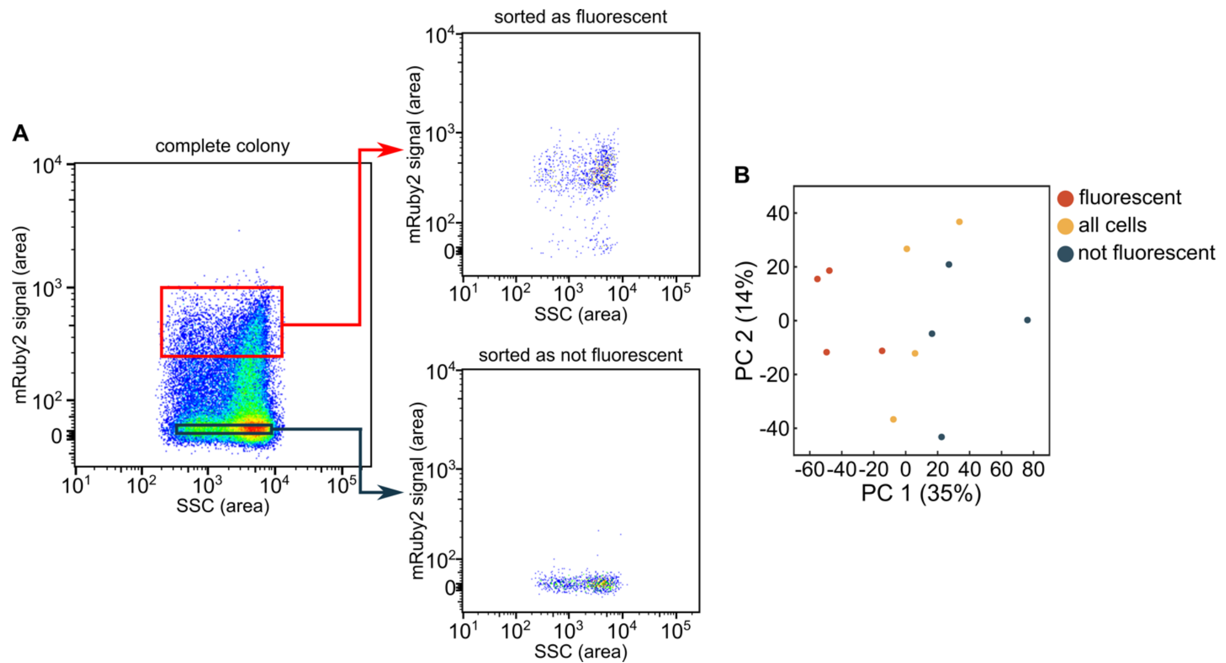

Figure S7. Application of flow cytometry with fluorescence-activated cell sorting to separate cells from the inner and outer regions of colonies. (*A*) Representative sorting results of a colony grown for 72 h, using the mRuby2 fluorescence signal and the side scatter (SSC) signal. Cells were sorted into two separate bins (red, black). (*B*) Principal component analysis of RNA-seq results of the two separated bins, or the entire population, from colonies that were grown for 72 h, showing the 1st (PC1) and 2nd (PC2) principal component axes. Each data point corresponds to an independent replicate ($n = 4$).

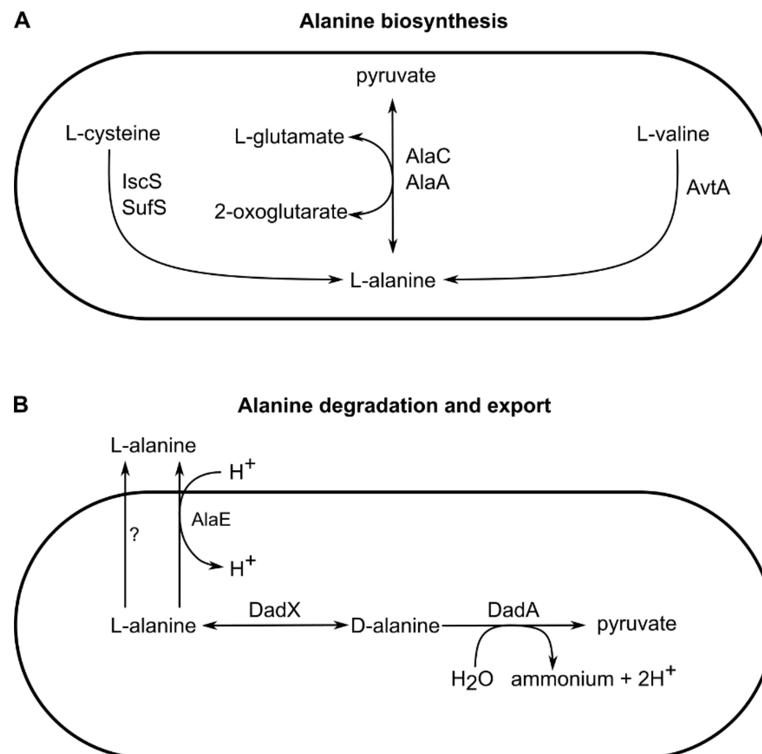

Figure S8. Key pathways in alanine metabolism. (*A*) Alanine biosynthesis pathways. (*B*) Alanine degradation and export pathways. Cells are drawn with a schematic rod shape.

bioRxiv preprint doi: https://doi.org/10.1101/2021.02.28.433255; this version posted February 28, 2021. The copyright holder for this preprint (which was not certified by peer review) is the author/funder, who has granted bioRxiv a license to display the preprint in perpetuity. It is made available under aCC-BY-NC-ND 4.0 International license.

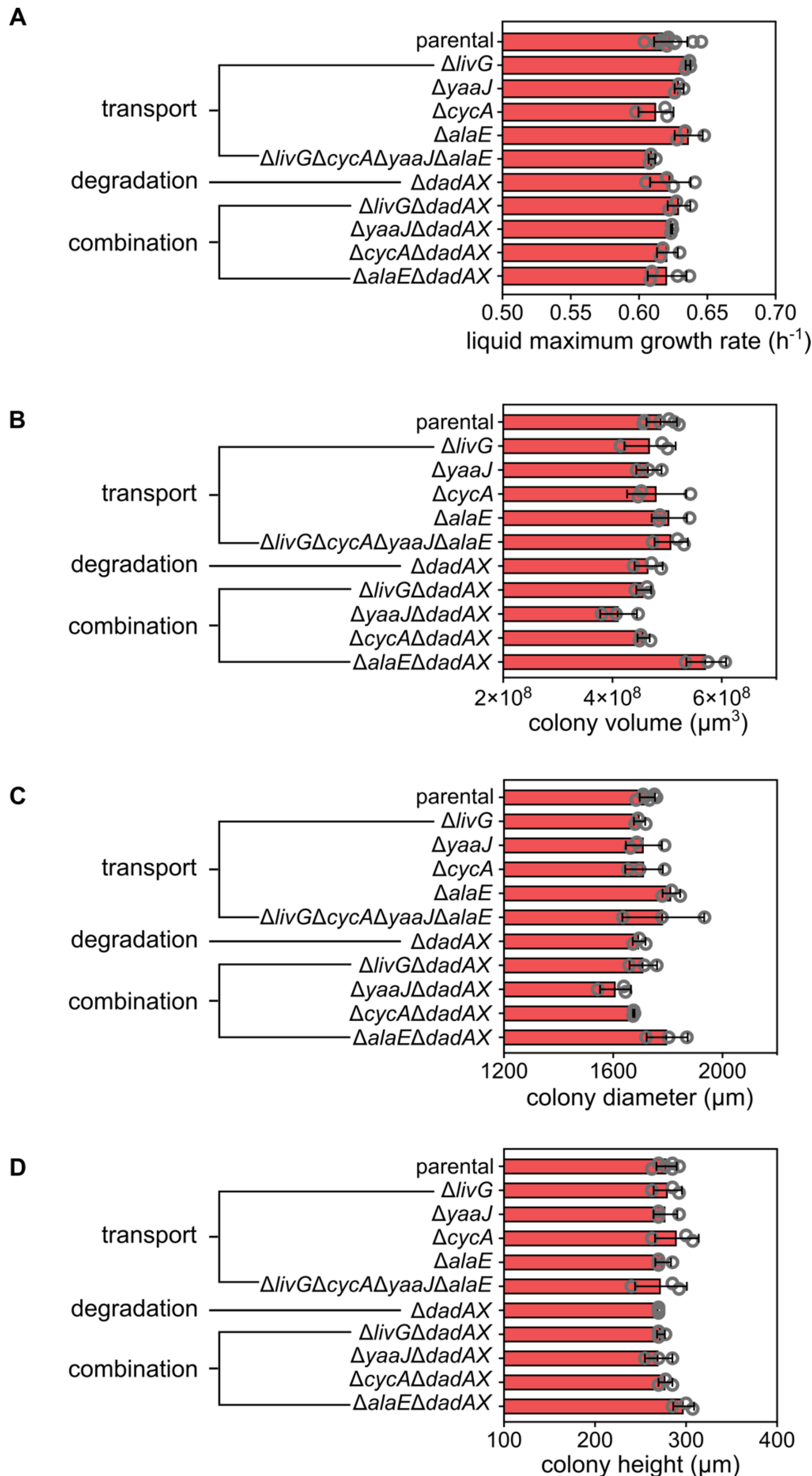

Figure S9. Growth rates and colony sizes for alanine metabolism mutants. (*A*) Maximum growth rate in liquid shaking cultures in M9 medium. Colony volume (*B*), diameter (*C*) and height (*D*) after 72 h of growth on M9 agar for different mutants in alanine transport and degradation, compared to the parental *E. coli* strain. Data are mean values ± s.d., each data point is shown as a grey circle.

bioRxiv preprint doi: https://doi.org/10.1101/2021.02.28.433255; this version posted February 28, 2021. The copyright holder for this preprint (which was not certified by peer review) is the author/funder, who has granted bioRxiv a license to display the preprint in perpetuity. It is made available under aCC-BY-NC-ND 4.0 International license.

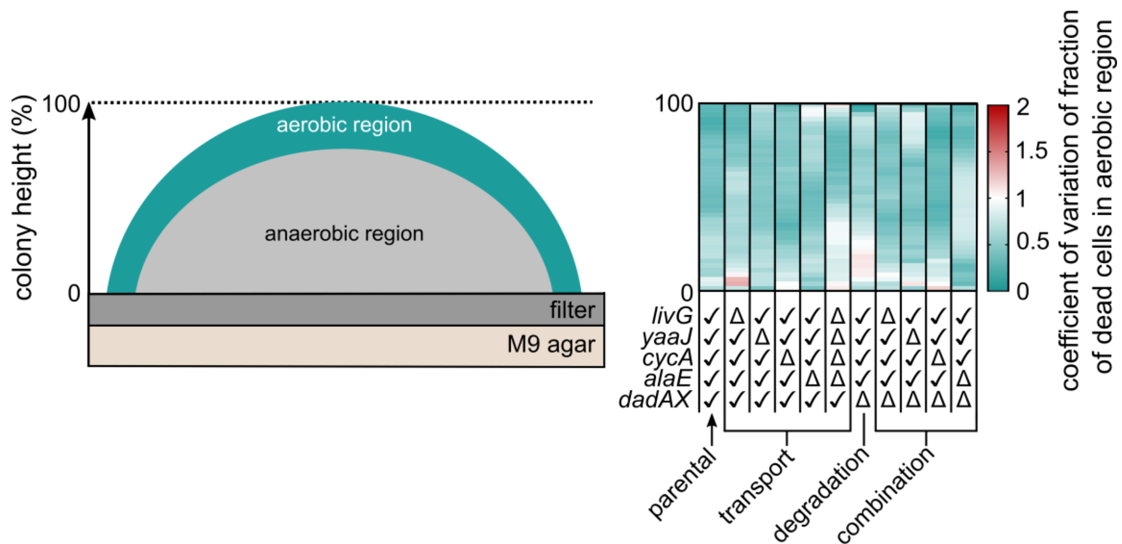

Figure S10. Coefficient of variation of the fraction of dead cells in the aerobic region of the colony. Heatmap shows the coefficient of variation for the data shown in Fig. 4A.

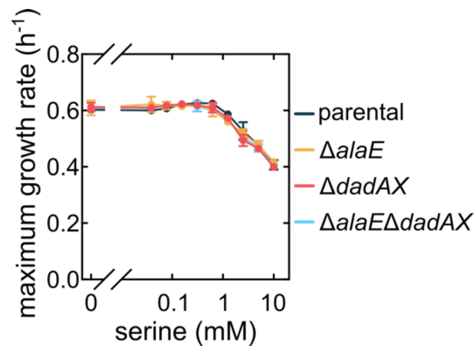

Figure S11. Effects of exogenously added alanine on maximum growth rate for alanine metabolism mutants are specific to alanine, and are not triggered serine. The maximum liquid culture growth rate as function of the concentration of exogenically added serine in M9 medium is the same for all strains. Data are mean values ± s.d., $n = 3$.

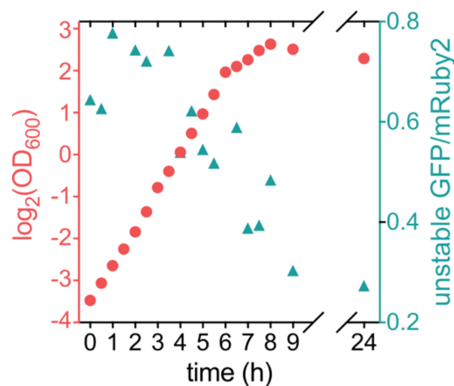

Figure S12. Ratio between unstable GFP and stable mRuby2 correlates with bacterial growth rate. Optical density at 600 nm (OD_{600}; shown in red, left y-axis) and the ratio between unstable GFP (with the ASV-tag) and mRuby2 (shown in green, right y-axis) as a function of time for a liquid culture of strain KDE2937.

bioRxiv preprint doi: https://doi.org/10.1101/2021.02.28.433255; this version posted February 28, 2021. The copyright holder for this preprint (which was not certified by peer review) is the author/funder, who has granted bioRxiv a license to display the preprint in perpetuity. It is made available under aCC-BY-NC-ND 4.0 International license.

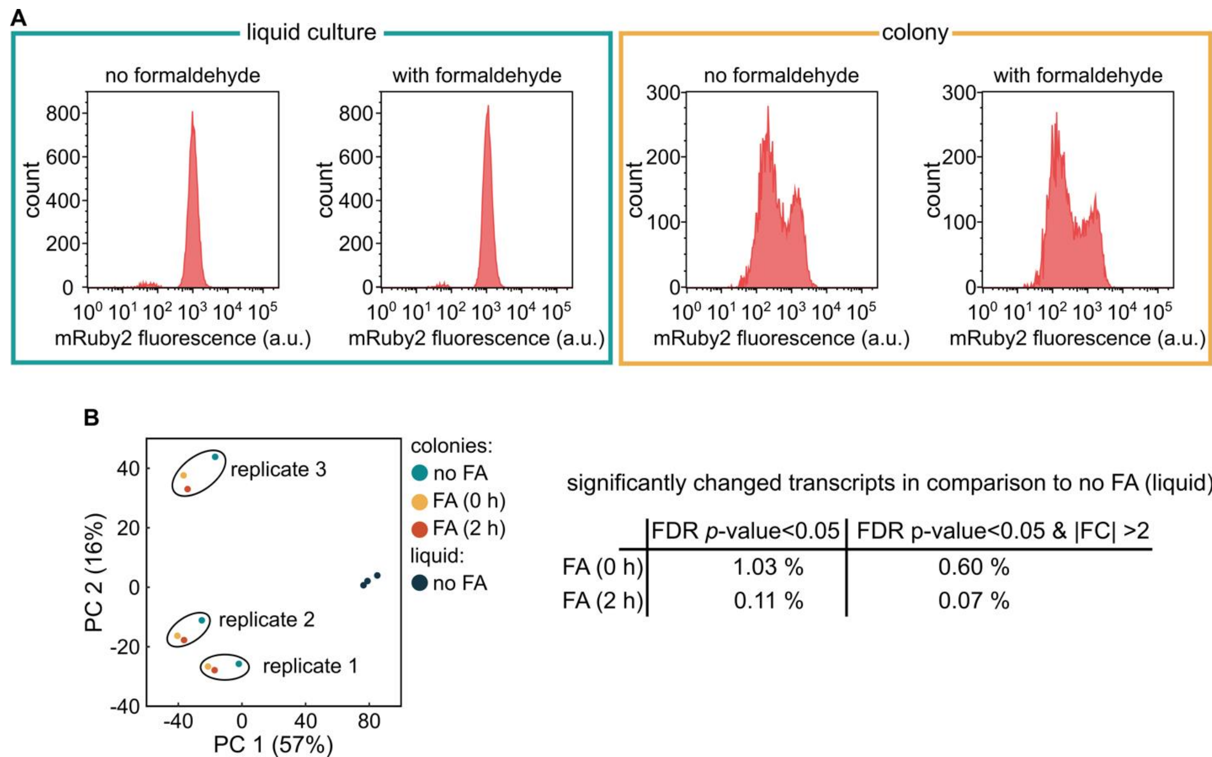

	FDR p-value<0.05	FDR p-value<0.05 & |FC| >2
FA (0 h)	1.03 %	0.60 %
FA (2 h)	0.11 %	0.07 %

Figure S13. Formaldehyde fixation does not affect mRuby2 fluorescence or the colony transcriptome. (*A*) Flow cytometry results for fluorescence of *E. coli* constitutively expressing mRuby2 (strain KDE722) with or without 2 hours of fixation using 4% formaldehyde. For the two panels on the left (enclosed by green box), the cells were grown in liquid shaking M9 medium. For the two panels on the right (enclosed by orange box), the cells were grown as a colony on M9 agar. (*B*) Principal component analysis of the transcriptomes of colonies grown for 72 h, which were either fixed with 4% formaldehyde (FA) for 0 h or 2 h, or without fixation. As a control, the transcriptome of cells from an exponentially growing M9 liquid shaking culture without fixation was also analyzed. Each data point corresponds to an independent replicate (n = 3). The table on the right indicates the number of differentially expressed genes in colonies, in comparison to the colonies without fixation, using as threshold for differentially expressed genes either a FDR-adjusted p-value < 0.05, or a FDR-adjusted p-value < 0.05 and an absolute fold-change (FC) > 2.

bioRxiv preprint doi: https://doi.org/10.1101/2021.02.28.433255; this version posted February 28, 2021. The copyright holder for this preprint (which was not certified by peer review) is the author/funder, who has granted bioRxiv a license to display the preprint in perpetuity. It is made available under aCC-BY-NC-ND 4.0 International license.

Table S1: Bacterial strains used in this study. Abbreviations: Kan = kanamycin. Superscript "R" = resistance. "-" = fusion. "::" = insertion. The scar corresponds to 5'-GAAGTTCCTATACTTTCTAGAGAATAGGAACTTC-3' sequence.

Strain	Genotype/ Relevant features	Reference
KDE261	*E. coli* strain carrying plasmid pCP20.	Drescher lab stock
KDE262	*E. coli* strain carrying plasmid pKD46.	Drescher lab stock
KDE264	*E. coli* strain carrying plasmid pKD3.	Drescher lab stock
KDE265	*E. coli* strain carrying plasmid pKD4.	Drescher lab stock
KDE1361	*E. coli* strain carrying plasmid pNUT1361.	Drescher lab stock
KDE2338	*E. coli* strain carrying plasmid pNUT2338.	Drescher lab stock
KDE2658	*E. coli* strain carrying plasmid pUC18R6KT-mini-Tn7-Km (Addgene #64969).	Drescher lab stock
KDE2659	*E. coli* strain carrying plasmid pTNS2 (Addgene #64968).	Drescher lab stock
KDE2674	*E. coli* strain carrying plasmid pNUT2674.	This study
KDE2787	*E. coli* strain carrying plasmid pNUT2787.	This study
KDE2838	*E. coli* strain carrying plasmid pNUT2838.	This study
KDE474	*E. coli* AR3110 WT.	Serra *et al.* (43)
KDE679	AR3110, P_{tac}-*mRuby2-mRuby2* and *Kan*^{R} inserted at *attB* site (P_{tac} without operator).	Vidakovic *et al.* (52)
KDE722	KDE679 with Δ*fliC*::scar.	Vidakovic *et al.* (52)
KDE1899	AR3110 with Δ*fliC*::scar.	This study
KDE2007	KDE679 with Δ*fliC*::scar, Δ*alaE*::scar.	This study
KDE2009	KDE679 with Δ*fliC*::scar, Δ*dadAX*::scar.	This study
KDE2086	KDE679 with Δ*fliC*::scar, Δ*alaE*::scar, Δ*dadAX*::scar.	This study
KDE2183	KDE679 with Δ*fliC*::scar, Δ*cycA*::scar.	This study
KDE2185	KDE679 with Δ*fliC*::scar, Δ*livG*::scar.	This study
KDE2438	KDE679 with Δ*fliC*::scar, Δ*yaaJ*::scar.	This study
KDE2533	KDE679 with Δ*fliC*::scar Δ*cycA*::scar, Δ*livG*::scar, Δ*alaE*::scar, Δ*yaaJ*::scar.	This study
KDE2564	KDE679 with Δ*fliC*::scar, Δ*cycA*::scar, Δ*dadAX*::scar.	This study
KDE2607	KDE679 with Δ*fliC*::scar, Δ*yaaJ*::scar, Δ*dadAX*::scar.	This study
KDE2937	KDE679 with Δ*fliC*::scar, P_{tac}-*sfgfp*(ASV) at the Tn7 insertion site, coding for an unstable superfolder GFP with an AANDENYAASV-tag.	This study
KDE2938	KDE679 with Δ*fliC*::scar, Δ*alaE*::scar, P_{tac}-*sfgfp*(ASV) at the Tn7 insertion site.	This study
KDE2939	KDE679 with Δ*fliC*::scar, Δ*dadAX*::scar, P_{tac}-*sfgfp*(ASV) at the Tn7 insertion site.	This study
KDE2940	KDE679 with Δ*fliC*::scar, Δ*alaE* Δ*dadAX*, P_{tac}-*sfgfp*(ASV) at the Tn7 insertion site.	This study

bioRxiv preprint doi: https://doi.org/10.1101/2021.02.28.433255; this version posted February 28, 2021. The copyright holder for this preprint (which was not certified by peer review) is the author/funder, who has granted bioRxiv a license to display the preprint in perpetuity. It is made available under aCC-BY-NC-ND 4.0 International license.

Table S2: Plasmids used in this study. Abbreviations: Kan = kanamycin, Amp = ampicillin, Chl = chloramphenicol. Superscript "R" = resistance. "-" = fusion.

Plasmid	Genotype/ Relevant features	Reference
pKD3	R6K ori, chloramphenicol acetyl transferase cassette flanked *by frt*, Amp^R.	Datsenko and Wanner (53)
pKD4	R6K ori, *T*n5 neomycin phosphotransferase cassette flanked *by frt*, Amp^R.	Datsenko and Wanner (53)
pKD46	Temperature sensitive replication origin oriR101, arabinose-inducible lambda recombinase genes, Amp^R.	Datsenko and Wanner (53)
pCP20	Temperature sensitive replication origin oriR101, Flp recombinase gene, Chl^R, Amp^R.	Cherepanov and Wackernagel (54)
pNUT1361	pSC101*, Kan^R, P_{tac}-*sfgfp*.	Drescher lab stock
pNUT2338	pSC101*, Kan^R, P_{tac}-*mRuby2-mRuby2*.	This study
pUC18R6KT-mini-Tn7-Km	R6K ori, contains *Tn7L* and *Tn7R* sites, between these sites a *T*n5 neomycin phosphotransferase cassette flanked *by frt*, Amp^R.	Choi *et. al.* (45), Addgene #64969
pTNS2	R6K ori, plasmid for transposase (*tnsABCD*) expression, Amp^R.	Choi *et. al.* (45), Addgene #64968
pNUT2674	pKD4 backbone, P_{tac}-*sfgfp*(ASV), coding for an unstable superfolder GFP with the AANDENYAASV-tag.	This study
pNUT2787	pUC18R6KT-mini-Tn7-Km backbone. Tn5 neomycin phosphotransferase cassette replaced by a chloramphenicol acetyl transferase cassette	This study
pNUT2838	pNUT2787 backbone. P_{tac}-*sfgfp*(ASV), coding for an unstable superfolder GFP with the AANDENYAASV-tag, placed between *Tn7L* and *Tn7R* sites.	This study

bioRxiv preprint doi: https://doi.org/10.1101/2021.02.28.433255; this version posted February 28, 2021. The copyright holder for this preprint (which was not certified by peer review) is the author/funder, who has granted bioRxiv a license to display the preprint in perpetuity. It is made available under aCC-BY-NC-ND 4.0 International license.

Table S3: DNA oligonucleotides used in this study.

Name	Sequence (5' to 3' direction)	Description
KDO834	ACAACTTTTTGTCTTTTTACCTTCCCGTTTCGCTCAAGTTAGTA TTTGACAATTAATCATCGGCTCGTATAATG	Insertions at the *attB* site
KDO894	TGGCTGTTTTTGAAAAAAATTCTAAAGGTTGTTTTACGACGTG TAGGCTGGAGCTGCTTC	*fliC* deletion
KDO895	AATCAGGTTACAACGATTAACCCTGCAGCAGAGACAGAACCT GCATATGAATATCCTCCTTAG	*fliC* deletion
KDO1662	TCCGGGCTATGAAATAGAAAAATGAATCCGTTGAAGCCTGCT TTTCATGGGAATTAGCCATGGTCC	Insertions at the *attB* site
KDO2562	CATCTCCATTAACATCCCATTACGCTTTTATTAAGGAGCATTA GCGTGTAGGCTGGAGCTGCTTC	*alaE* deletion
KDO2563	GCCAGTTAAAGACGCGACTGGCGATGCCAGTCGCGAAAAGA AGAGATGGGAATTAGCCATGGTCC	*alaE* deletion
KDO2566	TTAGATTATTATTCTTTTACTGTATCTACCGTTATCGGAGTGGC TGTGTAGGCTGGAGCTGCTTC	*dadAX* deletion
KDO2567	TTTTTGCACCCAGAAGACGTTGCCTCCGATCCGGCTTACAAC AAGATGGGAATTAGCCATGGTCC	*dadAX* deletion
KDO2845	CGTAGAGCCTGAACAACACAGACAGGTACAGGAAGAAAAAAA CGTGTAGGCTGGAGCTGCTTC	*cycA* deletion
KDO2846	CTAAAAGCTGGATGGCATTGCGCCATCCAGCATGATAATGCG GGGTCCATATGAATATCCTCCTTAG	*cycA* deletion
KDO2841	ACTGAAGCTGAAAAACGGCGCAGCGAAAGGAGAGCAGGCAT GATTGTGTAGGCTGGAGCTGCTTC	*livG* deletion
KDO2842	GGCGCTGACTTTGTCAAAGGACAACATGACTTTTTCCATCTTA GGTCCATATGAATATCCTCCTTAG	*livG* deletion
KDO3481	GTTTACACAGGAAAGTCATCGCGACCGGCAATAAGAGGGATA TGCGTGTAGGCTGGAGCTGCTTC	*yaaJ* deletion
KDO3482	GCCGACTTTAGCAAAAAATGAGAATGAGTTGATCGATAGTTGT GAATGGGAATTAGCCATGGTCCAT	*yaaJ* deletion
KDO3256	ACCTTTGCTAACCATCAACCACCTCCTTTAGTTTAATTAAGGT G	pNUT2338 construction
KDO3257	GTACCGCTAGCGGTGTAGGCTGGAGCTGCTTC	pNUT2338 construction
KDO3817	TCGACTCCTTCTCGAGGAATTCCTGCAGCC	pNUT2838 construction
KDO3818	GAATGCTGGTACCTCGCGAAGGCCT	pNUT2838 construction
KDO3785	TAGTTTTCATCGTTCGCGGCTTTATACAGTTCATCCATGCCGT GG	pNUT2674 construction
KDO3786	GCCGCGAACGATGAAAACTATGCCGCGAGCGTGTAAAGACA TGA	pNUT2674 construction
KDO4121	CGCTTGGACGGAAGAGTATGAGGATCCAACATTTC	pNUT2787 construction
KDO4121	CCAGATATCCGATCCTCATCCTGTCTCTTG	pNUT2787 construction
KDO4127	CGCGAGGTACCAGCATTCGCTTGGATTCTCACCAATGG	pNUT2838 construction